*diversity*

MDPI

*Article*

# Genome-Resolved Metagenomics of Microbes from the Atoud Dam, Southwestern Saudi Arabia

**Fatmah M. Alqahtani**

Department of Biology, College of Science, King Khalid University, Abha 61413, Saudi Arabia; mhussen@kku.edu.sa

**Abstract**

Artificial freshwater bodies receive elemental inputs and face environmental stressors, posing a risk of wetland pollution that could threaten ecological health. In such an inland backwater, its microbial diversity and functional potentials remain uncharacterized. Here, shotgun metagenomic sequencing was performed on environmental DNA samples collected from the Atoud Dam reservoir in southwestern Saudi Arabia. The taxonomic assignments of the sequencing reads identified *Pseudomonadota* and *Actinomycetota* as the dominant phyla, while the most prevalent species was *Microcystis aeruginosa*. Binning assembled contigs recovered 30 metagenome-assembled genomes representing 11 phyla, suggesting potentially novel bacterial taxa and metabolic functions. Functional analysis of gene-coding sequences identified genes associated with mobile genetic elements and xenobiotic biodegradation pathways as the main factors driving the spread of antibiotic resistance genes. Additionally, a community-wide analysis of enzyme-encoding genes involved in regulating the carbon, nitrogen, and sulfur cycles revealed significant annotation of denitrification and thiosulfate oxidation pathways under anoxic conditions, suggesting early signs of eutrophication and a potential risk of algal blooms. Overall, our study provides detailed insights into the genomic capabilities of the microbial community in this previously understudied ecosystem and establishes baseline data for future assessments of microbial biodiversity in other, less-explored ecosystems, thereby facilitating more effective biomonitoring and discovery.

**Keywords:** freshwater; metagenomics; microbial biodiversity; antibiotic resistance genes; metagenome-assembled genomes; biogeochemical cycling



Academic Editor: Michael Wink

Received: 2 December 2025
Revised: 23 December 2025
Accepted: 23 December 2025
Published: 25 December 2025



## 1. Introduction

To secure water needs, especially in regions prone to prolonged droughts, artificial freshwater storage systems are built by damming rain runoff to serve as environmental freshwater reservoirs. While managing freshwater flow can provide a valuable resource for irrigation and agriculture, disrupting the natural flow can cause ecological changes by trapping sediments, which can lead to eutrophication and the formation of wetlands [1]. The Atoud Dam reservoir is located in the Asir Province of southwestern Saudi Arabia at an elevation of approximately 1850 m above sea level. It was built in 1994 to reduce the risk of flooding during unexpected heavy rainfalls. The Atoud Dam is situated downstream of large agricultural areas and has recently been surrounded by urban districts, making it an ecologically sensitive freshwater system and increasing its vulnerability to environmental stress. The dam is originally a semi-closed system, and with long-term increases in

global warming and less precipitation, there is no natural flushing or dilution of nutrients or pollutants.

The key components of aquatic ecosystems are microbes, which possess a diverse array of metabolic genes and serve as the main drivers of biogeochemical cycling [2]. In fact, ecosystem health can be assessed by analyzing the phylogenetic and functional assemblages of a microbial community, which are considered the most sensitive indicators of ecosystem health. Unlike marine environments, few studies have been conducted on function-based metagenomics screenings of inland aquatic resources [3]. Although freshwater aquatic ecosystems cover only about 2.8% of the Earth's surface [4], their diverse microbial communities accelerate nutrient cycling by metabolizing organic and inorganic compounds, thereby shaping the biogeochemical characteristics of sediments [5]. In other words, microorganisms control carbon cycling [6], drive nitrogen-transforming networks [7], and facilitate sulfate-driven remineralization [8], making freshwater aquatic ecosystems hotspots of biogeochemical activity.

Genome-resolved metagenomics is an independent-culture approach that links microbial function to taxonomy, revealing a specialized microbial ecology that is metabolically related to their environmental conditions [9]. Metagenomic profiling, as a rapid and advanced technique, provides comprehensive insights into environmental biodiversity and has been extensively used as a tool for biomonitoring assessments. For example, it has been used to assess aquatic health status [10], evaluate biodiversity across seasonal patterns [11], monitor pollution and antibiotic-resistant proliferation [3], and even continuously recover genomes of previously undescribed microbial species from environmental DNA (eDNA) samples [12]. The use of eDNA and high-throughput DNA sequencing techniques in biodiversity and biomonitoring studies has gained popularity in developed countries for over two decades. However, local factors can explain the limited usage of this technique in understudied environments, including a lack of technical expertise, the high cost involved in DNA sequencing, and, most importantly, the absence of regional DNA reference datasets, especially from unexplored ecosystems [13].

Nevertheless, Saudi Arabia's ecosystems remain among the most understudied environments globally in terms of microbial diversity and their metabolic potentials. Therefore, the main goal of this study is to identify the structure of the microbial community at the Atoud Dam and its metabolic capabilities using a genome-resolved metagenomics approach, thereby uncovering previously unknown microbial biodiversity and elucidating their environmental roles. In this study, (1) the microbial community structure and abundance in the water surfaces and sediments of the Atoud Dam were characterized through taxonomic classification of sequencing reads, (2) metagenome-assembled genomes (MAGs) were recovered and taxonomically classified through phylogenetic analysis, and, finally, (3) the recovered MAGs were functionally annotated to detect antibiotic-resistant and pollutant-degrading genes, as well as functional genes involved in regulating carbon, nitrogen, and sulfur cycles. The microbial community profiling and metabolic pathway annotations indicate a potential influence of environmental factors on the biogeochemical cycles in the Atoud Dam, suggesting eutrophication.

## 2. Materials and Methods

### 2.1. Sample Collection

In this study, an important urban wetland ecosystem that had not been previously studied was selected. The Atoud Dam (18.260571° N, 42.716227° E) is a small, shallow reservoir that drains into the Atoud Valley, with an estimated watershed area of 10 $km^2$. Four samples were collected in January 2024, during the peak of the dry season, from different sites spaced approximately 100 m apart along the southern shoreline of the Atoud

Dam's waterbody, due to accessibility (Figure S1), at a depth of approximately 20 cm. Each sample consisted of approximately 10 mL of surface water and a small portion of sediments, collected in 15 mL sterile centrifuge tubes. The sample tubes were carefully packed, placed in an icebox, and kept frozen at −20 °C until total eDNA extraction was performed in the lab within 24 h.

### *2.2. eDNA Extraction and Sequencing*

After completely thawing the samples, the sample tubes, containing surface water and sediments, were thoroughly and gently mixed using a vortex. After centrifuging the 15 mL sample tubes for 10 min at 1000 rpm, the pellets from each sample were divided into two subsamples (0.5 g each) to increase DNA yield. Metagenomic DNA was extracted using a DNeasy PowerBiofilm kit (QIAGEN, Hilden, Germany) according to the manufacturer's instructions, with minor modifications. In the bead-beating step, cells were disrupted in a homogenizer with three cycles of beating and freezing for 40 s each. Then, the extracts from the subsamples were combined for each sample into a single spin column for the DNA clean-up steps. The quantification and quality of the collective DNA samples were examined using a NanoDrop Spectrophotometer, and the integrity of each sample was examined using agarose gel electrophoresis. A NEBNext Ultra II DNA Library Prep Kit for Illumina (New England Biolabs, Ipswich, MA, USA) was used for library construction. The constructed indexed shotgun metagenomic libraries were sequenced to generate paired-end reads (2 × 150 bp) on the Illumina NextSeq 2000 (Illumina Inc., San Diego, CA, USA).

### *2.3. Bioinformatics Workflow*

A total of raw sequence reads (22.7 Gbp) were generated and filtered first using Cutadapt and KneadData to remove irrelevant sequences (such as adapter sequences, primers, or poly-A tails) and host sequences, respectively [14,15]. Afterward, 96.3% of the filtered reads were assessed for quality using FastQC [16]. *K*-mer-based taxonomic assignment was carried out using Kraken2 with parameters (minimum number of overlapping *k*-mers = three and a confidence threshold for classification $\leq$ 0.05) against the PlusPF (2024) database, as well as the fungal genome and viral genome (2019) databases [17]. The abundance of each taxonomic rank for each microbial group was estimated with Bracken [18]. Concurrently, clean reads from all samples were co-assembled using the de novo metagenomic assembler MEGAHIT with default parameters [19]; subsequently, the assembled contigs were evaluated for assembly quality with metaQUAST [20].

Then, the assembled contigs were clustered into metagenomic bins using the binning modules (MetaBAT2, MaxBin2, and CONCOCT), followed by refinement with the bin refinement module (MetaWRAP) [21]. For each binned MAG, redundancy was addressed using dRep [22], while completeness and contamination were estimated with CheckM2 [23]. The abundance matrices of each MAG, defined as the number of mapped reads divided by the total number of filtered reads in the metagenome, were then evaluated using HISAT2 [24]. The MAGs were taxonomically classified using the gtdbtk classify-wf module from the GTDB-tk database [25]. Phylogenetic analysis was performed by constructing a maximum likelihood tree that compared the MAGs with a subset of COG (Clusters of Orthologous Groups) domains, selected based on alignment similarity using the "insert genome into species tree" function on the Kbase platform [26]. Open reading frames (ORFs) were predicted via the Rapid Annotation using Subsystems Technology (RAST-tk) database [27]. Antibiotic resistance genes were identified by aligning the ORFs against the GhostKOALA database, an automatic annotation and KEGG mapping server for metagenomes [28]. MAGs were functionally annotated for metabolic functions and biogeochemical cycles using the Distilled and Refined Annotation of Metabolism (DRAM)

tool, which inferred metabolic descriptors for each MAG based on functional marker genes using multiple databases [29].

## 3. Results and Discussion

### *3.1. Taxonomic Classification of Metagenomic Data*

The metagenomic shotgun sequencing reads yielded a total of 144,561,992 high-quality reads (150–151 base pairs long, with 62% GC content) after quality filtering. Out of these, 18,824,633 sequences (13.02%) were classified as microbial reads. Biodiversity across the four samples was assessed by analyzing alpha diversity metrics (Figure 1a), which revealed a large number of observed species and minor differences among the samples. For instance, the Shannon diversity index was about 0.7, suggesting universality in the microbial community's diversity and evenness throughout the Atoud Dam samples. Additionally, the Simpson index was approximately 0.99, signifying a balanced community structure without significant dominance. The Inverse Shannon indicated a microbial community with a high number of species and an even distribution, thus suggesting a highly diverse ecosystem. The abundances of the top 38 phyla are shown in Figure 1b. The most dominant phyla were *Pseudomonadota* and *Actinomycetota*, followed by *Myxococcota*, *Planctomycetota*, *Bacteroidota*, *Cyanobacteriota*, *Acidobacteriota*, *Bacillota*, and *Verrucomicrobiota*. The next prominent group included the archaeal phylum (*Euryarchaeota*), along with *Deinococcota*, *Chloroflexota*, *Gemmatimonadota*, the fungal phylum (Ascomycota), and *Nitrospirota*.

To better visualize the diversity of microbial groups, their abundances, and confidence levels, an interactive hierarchical classification was created using a classification assignment pool for all four samples (File S1). Of all sequence reads, 12.3% were taxonomically assigned. Among these assigned reads, 99.4% were classified as bacteria, followed by eukaryota (0.04%), archaea (0.03%), and viruses (0.005%) (Figure 1c). Additionally, the richness metrics of taxonomic features (richness/OTU-like profiles derived from read-based classification) were calculated for each microbial group. A total of 1078 unique taxonomic features were identified across 6870 total observations (ranging from 37 to 450) (Figure 1d). Good's coverage was estimated based on the proportion of singleton taxonomic features relative to the total number of observations across all four samples and averaged 89.13%, indicating that the assigned sequences provide a good representation of the microbial communities present in the metagenomic samples. In addition, the taxon composition of the microbial community was clustered based on relative abundance using Bracken. A minimum threshold of 10 Kraken reads was set to include a classification in the final abundance estimate for each taxon of bacteria, fungi, protists, archaea, and viruses. Comparing the percentage composition of phyla across all microbial groups revealed that bacterial phyla were dominant, accounting for 72.06% of the total phylum-level assignments in the sample (Figure 1e). In addition, among bacterial taxonomic assignments, 71.23% of the sequence reads were classified at the species level, indicating that bacteria were predominantly represented at the species level in the read-based classification.

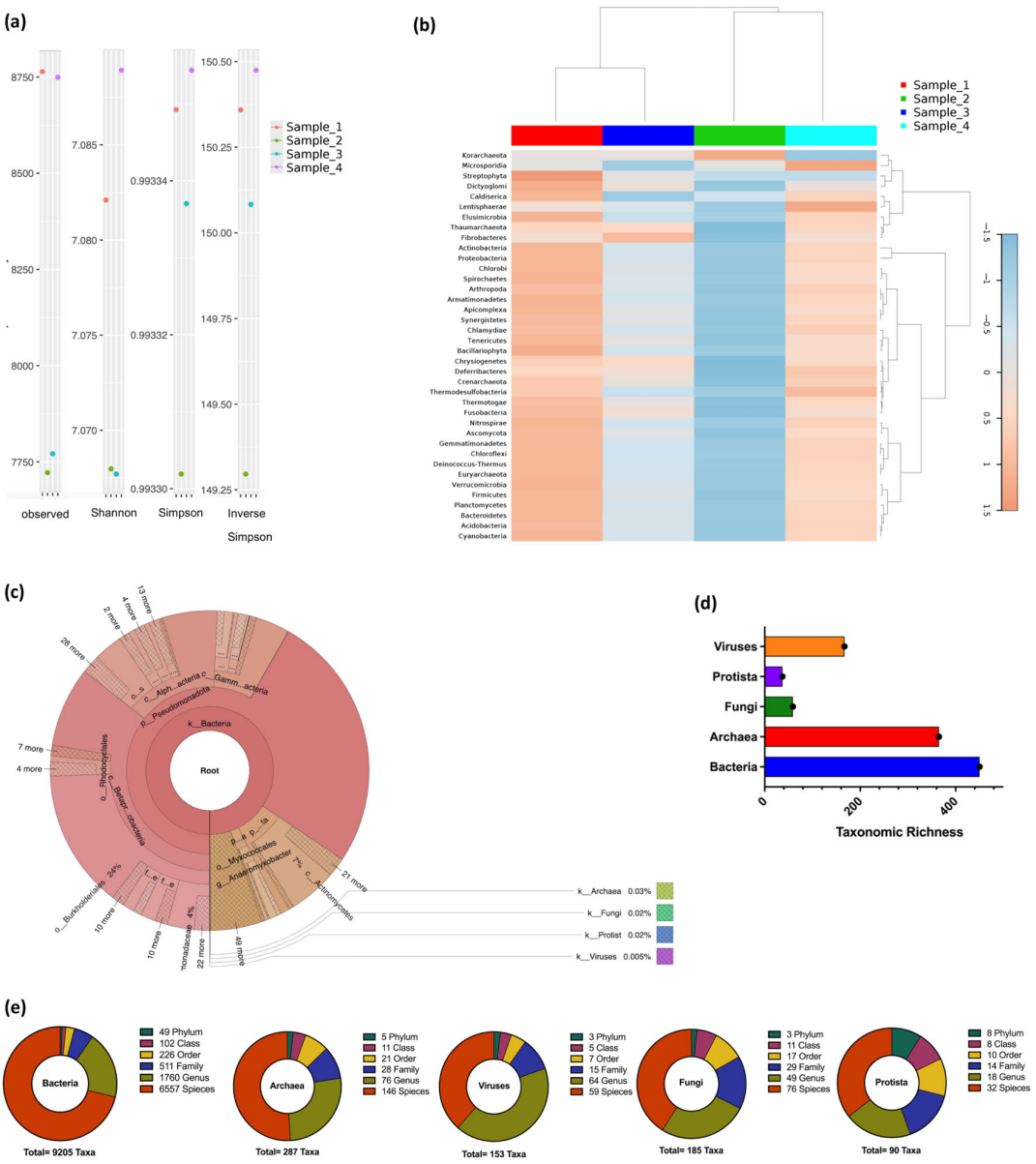


**Figure 1.** Microbial community composition of environmental samples from Atoud Dam. (**a**) Dot plots of alpha diversity using phyloseq parameters [30] to calculate Observed, Shannon, Simpson, and Inverse Simpson metrics for each sample. (**b**) Clustered heatmap visualizing phylum-level composition across samples. The warmer the color, the higher the abundance; the cooler the color, the lower the abundance. (**c**) Hierarchical data at all taxonomic levels for bacteria, archaea, viruses, and eukaryotes, estimated with Kraken2 and visualized using the Krona metagenomic tool [31]. (**d**) Number of unique taxonomic features (taxonomic richness) among microbial groups. (**e**) Donut charts illustrating the relative abundances of different taxonomic ranks, estimated with Bracken across bacteria, archaea, viruses, fungi, and protists.

### *3.2. Microbial Community Structure*

The assigned reads for the bacterial domain were represented using Sankey networks to depict the abundance estimates across phyla, classes, orders, families, genera, and species. The *Pseudomonadota* (*Proteobacteria*) phylum dominated the sample, accounting for 78.45% (Figure 2a). Although it is often associated with anthropogenic interference and sewage contamination in freshwater samples [32,33], the high prevalence and variability of these bacteria can serve as indicators of nutrient enrichment [34]. *Pseudomonadota* were also dominated by their classes. The abundance of *Betaproteobacteria* was significantly higher (59.2%)

among other bacterial classes, followed by *Alphaproteobacteria* (20.5%), *Gammaproteobacteria* (9.4%), and *Deltaproteobacteria* (3.9%). Other less abundant classes within *Pseudomonadota* were also represented, such as *Acidithiobacillia* (0.02%), *Hydrogenophillia* (0.0008%), and *Zetaproteobacteria* (0.0007%). Despite *E. coli* being a notoriously sensitive indicator of fecal contamination in freshwater bodies, the relative abundance of this bacterium was significantly low in the sample. In fact, other genera within *Pseudomonadota* were the most abundant, including *Pseudomonas*, *Variovorax*, *Bradyrhizobium*, *Thermomonas*, *Hydrogenophaga*, and *Sphingomonas*. Some of these genera play ecological roles in bioremediation (*Pseudomonas* [35], *Variovorax* [36], *Hydrogenophaga* [37], and *Sphingomonas* [38]) and the nitrogen cycle (*Bradyrhizobium* [39] and *Thermomonas* [40]).

The second most abundant class, not belonging to the *Pseudomonadota*, was *Actinomycetota* (4.0%), representing the second most abundant phylum, *Actinomycetota* (12.0%). This phylum is found in almost all freshwater environments, cohabiting with primary producers and mediating most heterotrophic activities [41]. The most abundant genus within the *Actinomycetota* phylum was *Streptomyces*, a freshwater sediment inhabitant that contributes to the breakdown of organic materials and helps control cyanobacterial blooms through the production of secondary metabolites [42]. *Mycobacterium* was also the second most abundant genus in this phylum, forming biofilms with the capacity for oligotrophic adaptation and possessing pathogenic potential in aquaculture [43]. The third most abundant phylum was *Myxococcota* (2.09%), naturally associated with soil and freshwater ecosystems. The member of this phylum, *Anaeromyxobacter*, was the most prevalent genus in the entire sample, residing in freshwater sediments and playing an essential role in nitrogen cycling [44] and in the reduction of radionuclides such as uranium (U) and technetium (Tc) [45].

The phyla *Cyanobacteria*, *Planctomycetota*, *Bacteroidota*, *Acidobacteriota*, *Verrucomicrobiota*, *Thermodesulfobacteriota*, *Bacillota*, *Gemmatimonadota*, and *Nitrospirota* ranged from 1.5% to 0,05% of the assigned reads. Representing the *Cyanobacteria* phylum, the toxigenic *Microcystis aeruginosa* dominates significantly (4.52%) among the assigned reads at the species level. *M. aeruginosa* is famously known for causing destructive, harmful algal blooms, such as those documented in Lake Erie [46] and Lake Okeechobee [47] by producing the potent hepatotoxin microcystin, which is commonly recognized as a cyanotoxin in freshwater ecosystems [48]. During the peak blooming season, especially in summer, *M. aeruginosa* can account for up to 76.6% of metagenomic reads [49]. Another study found that increasing nutrient loads can proportionally raise the relative abundance of *M. aeruginosa* from 1.44% to 41.76% [50]. The second most abundant species among the assigned reads was *Luteitalea* sp. TBR-22, which belongs to the *Acidobacteriota* phylum, a group of bacteria known for their symbiotic relationship with plants in aquatic environments. *Luteitalea* sp. TBR-22 was first isolated in Japan (2022) from wild duckweeds, which are freshwater plants [51]. Overall, the taxonomic classification of metagenomic sequences revealed the composition of typical freshwater bacterial communities, characterized by higher abundances of *Pseudomonadota* and *Actinomycetota*, along with other low-prevalence bacteria.

Based on the OUT/richness chart, the second most abundant domain after bacteria was archaea. In the present dataset, eight phyla were identified within the Archaea (Figure 2b). The phyla assigned to archaea were also represented using Sankey networks based on abundance estimates. *Euryarchaeota* had the highest abundance, followed by *Nitrososphaerota* (*Thaumarchaeota*), *Thermoproteota* (*Crenarchaeota*), *Candidatus Korarchaeota*, *Candidatus Poseidoniota* (*Thermoplasmatota*), *Candidatus Nanohaloarchaeota*, and *Candidatus Lokiarchaeota*. The relative abundance of the phyla *Euryarchaeota*, *Nitrososphaerota*, and *Thermoproteota* was estimated at 93.82%, 2.195%, and 1.179%, respectively. *Euryarchaeota* is the most diverse phylum within the Archaea domain, including methanogens and halophiles. Within the class *Halobacteria*, *Natrialbaceae* is the only family in the order *Natrialbales*. *Na-*

*trialbaceae* mainly consists of obligately alkaliphilic members that grow in alkaline (pH > 8), high-salt environments. *Salinadaptatus halalkaliphilus*, the most abundant species in the archaeal group (35.37%), was first isolated from a salt pond in China (2021) and exhibits strictly aerobic metabolism and growth under haloalkaliphilic conditions [52].

In viruses, the order *Caudovirales* led with the highest assigned sequences in the viral genomes, with a relative abundance of about 99.38% in total viral diversity, followed by the orders *Herpesvirales* and *Ortervirales* (Figure 2c). In addition, another important viral family, *Baculiviridae*, of invertebrate host origin, was identified. *Choristoneura fumiferana* granulovirus (ChfuGV) is a species of insect virus that infects and kills the eastern spruce budworm, *Choristoneura fumiferana*. This virus is a member of the *Betabaculovirus* genus within the *Baculoviridae* family, and it is a promising candidate for use as a biological insecticide to control the spruce budworm, a major forestry pest in North America [53].

Within eukaryotes, more than 10 assigned phyla emerged (Figure 2d,e). Based on abundance, the phylum Ascomycota was the most abundant, followed by Basidiomycota. After fungal phyla, the frequently assigned phyla in eukaryotes were Bacillariophyta, Apicomplexa, Euglenozoa, Evosea, Cercozoa, Heterolobosea, and Fornicota. The taxon details across the major domains and viruses are provided in the Supplementary Materials (Table S1).

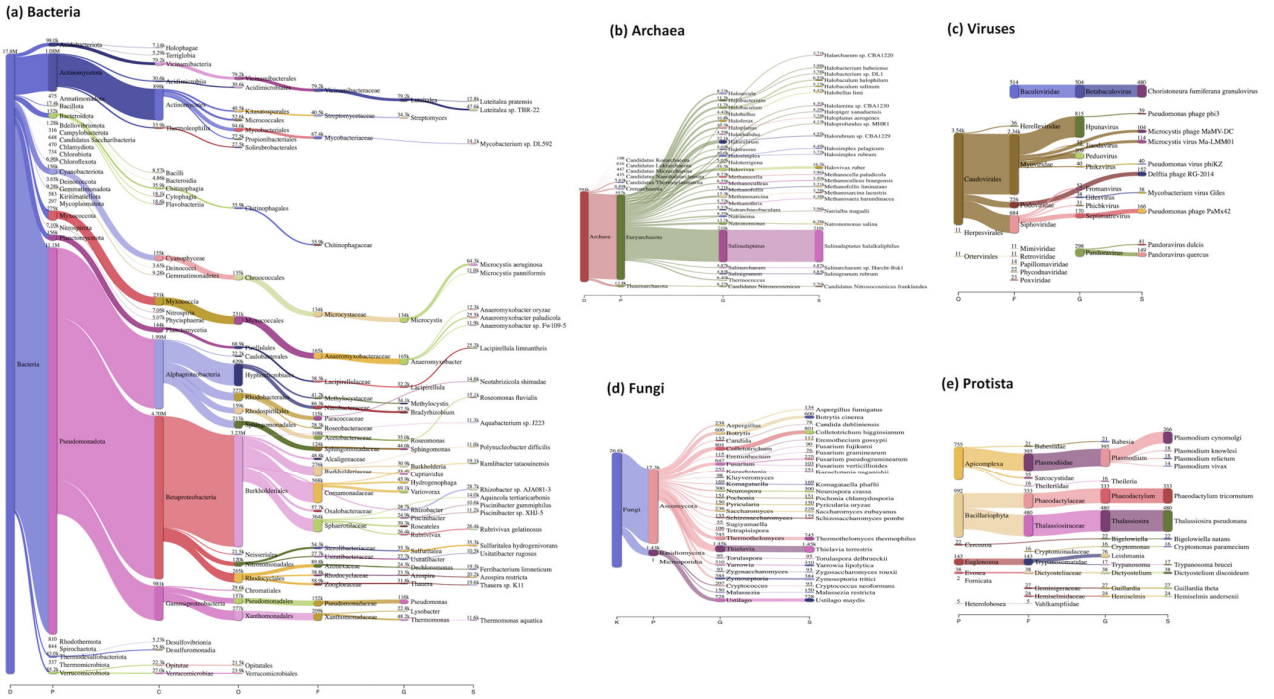


**Figure 2.** Sankey diagrams generated via the Pavian tool [54] using the total number of assigned reads that were estimated with Kraken2 for (**a**) the bacterial domain at the levels of phylum, class, order, family, genus, and species and for (**b**) the archaeal domain, (**c**) viruses, (**d**) fungi, and (**e**) protists at only the four different levels of taxonomic ranks to simplify the charts.

### *3.3. Construction of MAGs*

The co-assembly of the Atoud Dam paired-end reads generated a total of 756,412 contigs with an N50 of 8759 bp, a total length of 842,973,317 bp, a 64.45% mapping rate, and an average coverage depth of 14×, based on the assembly quality assessment tool metaQuast. Binning and refinement were performed with the metaWRAP binning module, resulting in 6 high-quality bins with over 90% genome completeness, <5% genome contamination, and 24 medium-quality bins (>50% completeness, <10% contamination). All MAGs were checked and dereplicated for quality and redundancy using CheckM2 and dRep, respec-

tively. The initial phylogenomic context of the 30 MAGs was investigated using CheckM2, which identified representatives of 11 prokaryotic phyla; a single MAG was assigned to archaea, while the rest were assigned to bacteria. To further improve the taxonomic resolution of the MAGs classification, taxonomic assignments were obtained using GTDB-Tk (Table S2). Additionally, a comprehensive phylogenetic approach was used to construct a phylogenetic tree from a set of Clusters of Orthologous Groups (COG)-associated proteins, providing a phylogenetic approximation of species placement (Figure 3a).

Seven MAGs were placed into the phylum *Pseudomonadota*, including the families of *Usitatibacteraceae*, *Burkholderiaceae*, *Acetobacteraceae*, and *GCA-2729495*, with the highest relative abundance of 3.6% among all MAGs (Figure 3b) according to the collective mapped reads of all *Pseudomonadotal* bins. The phylum *Verrucomicrobiota* followed with six MAGs, primarily represented by the families *Akkermansiaceae*, *V1-33*, *JACRJZ01*, *Palsa-1439*, *JAHDYP01*, and *CAITUY01*, with a total relative abundance of 1.5%. Four core phyla were *Myxococcota* (3 MAGs, 1.45%), *Bacteroidota* (3 MAGs, 1.3%), *Planctomycetota* (3 MAGs, 0.9%), and *Bdellovibrionota* (3 MAGs, 0.23%). Additionally, four of the MAGs were classified within the bacterial phyla *Chloroflexota* (0.336%), *Gemmatimonadota* (0.298%), *Nitrospirota* (0.145%), and *Acidobacteriota* (0.59%), as well as the archaeal phylum *Diapherotrites* (*Candidatus* Iainarchaeota) (0.038%). Notably, according to gtdbtk.bac120.red_dictionary (the classification based on a set of 120 bacterial phylogenetic markers), one MAG (bin.3), a member of *Bdellovibrionota*, could represent a potentially novel bacterial genus based on relative evolutionary distance (RED). In addition, ten MAGs that could represent potentially novel bacterial species were also identified based on (RED) values (Table S2). The potential novel species of these MAGs belonged primarily to the *Verrucomicrobiota*, *Pseudomonadota*, *Bdellovibrionota*, *Planctomycetota*, and *Chloroflexota*.

Despite the varying degrees of completeness among the MAGs, genome completeness was not significantly correlated with the number of coding genes in each recovered MAG (correlation coefficient = −0.023, $p$-value = 0.903) or with genome size (correlation coefficient = 0.147, $p$-value = 0.437). However, the correlation between genome completeness and GC content and N50 contig showed different levels of significance (Figure 3c). While GC content can be mainly influenced by the organism's phylogeny and its nonuniformity across all taxa [55], the N50 contig is heavily affected by the inherent limitations of short sequence reads. These limitations are further complicated by difficulties in assembling repetitive sequences, mobilization events, and horizontal gene transfers, especially if the sample represents an environmentally complex microbial community, unlike the less complex fecal microbiome sample [56]. Nonetheless, the average coding density of all our MAGs was (0.91) high enough to allow functional comparisons among these MAGs.

### *3.4. Antibiotic Resistance Genes (ARGs)*

A total of 22,607 contigs were generated from the Atoud Dam MAG dataset. From these contigs, a total of 119,557 coding genes were identified, and the translated protein sequences of these genes were used as a query dataset to characterize the functional annotation of the MAGs for antibiotic resistance using GhostKOALA. Approximately 698 query entries were annotated as genes involved in drug resistance, including those related to antimicrobials. Of these, β-lactam resistance was the highest, followed by cationic antimicrobial peptide (CAMP) resistance and vancomycin resistance (Figure 4a and Table S3). Among the ARGs directly involved in β-lactam resistance, multidrug efflux pump genes (*acrA*, *acrB*, and *tolC*) are frequently detected in freshwater metagenomes, forming the AcrAB-TolC efflux pump system, which confers increased tolerance to biocides. This type of resistance mechanism helps bacteria expel toxic compounds, including β-lactams [58]. In addition, other genes involved directly in β-lactam resistance were annotated, including *AmpC*, *bla*2, *blaOXA*-10,

and *oxa* (β-lactamase enzymes that hydrolyze β-lactam antibiotics), *AmpG* (a peptidoglycan recycler and β-lactamase inducer), *blaI* and *NagZ* (a β-lactamase enzyme regulators), *blaR1* (a β-lactam antibiotic sensor), *CpxR* and *oprM* (efflux pump regulators), and *ftsI* and *penP* (mutations in these genes can produce a penicillin-binding protein 3 (PBP3) alteration) [59]. In aquatic ecosystems, the majority of ARGs documented with high frequency worldwide are those related to β-lactam resistance [3]. Even in freshwater ecosystems with a low rate of anthropogenic impact, the natural presence of antimicrobial resistance was detected with high prevalence, primarily attributed to β-lactam resistance [60]. Concordantly, the functional protein domain profile across the MAG library demonstrated the frequency of β-lactamase in 69.5% of MAGs (Figure 4b) with a total of 35 hits, thereby emphasizing the risk of natural occurrence and distribution of β-lactam resistance.

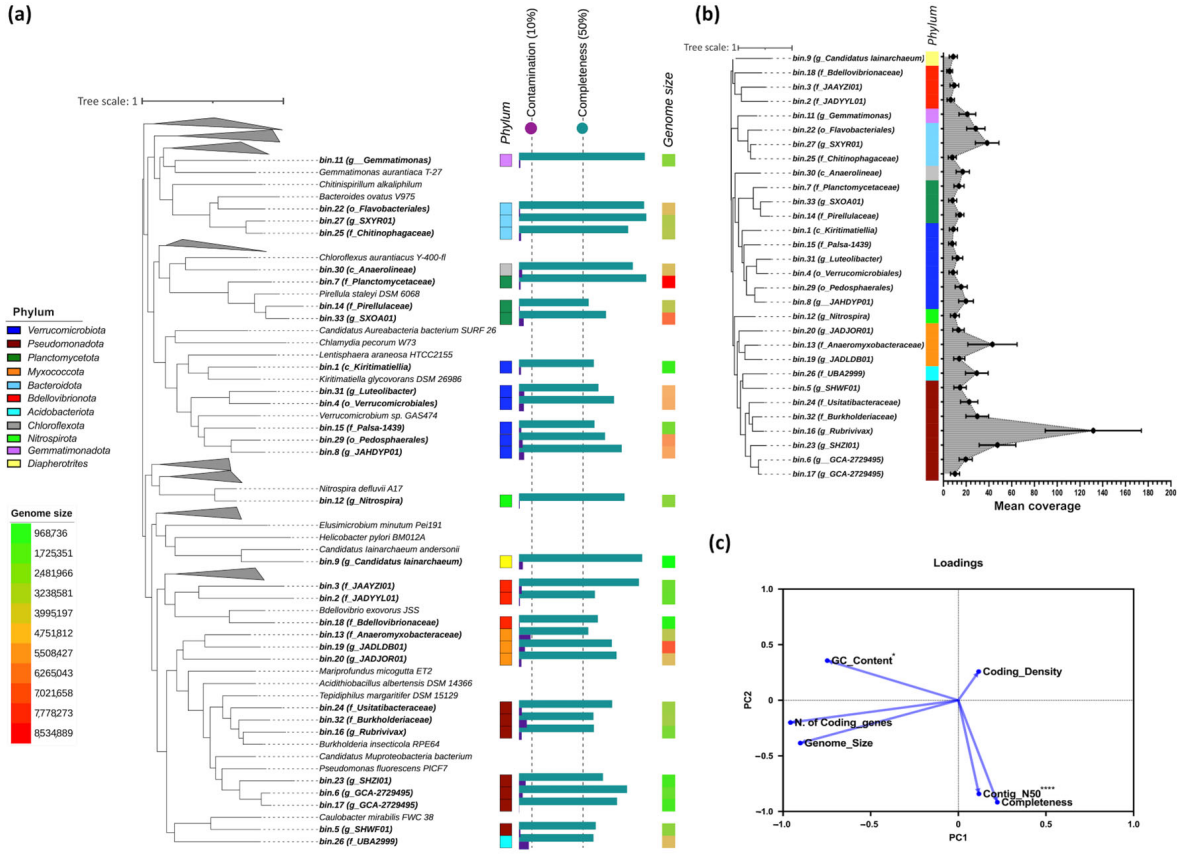


**Figure 3.** Taxonomic composition of the recovered Atoud Dam MAGs. (**a**) Phylogenetic tree of MAGs based on RAST-annotated genomes with a set of representative genomes and COG-associated proteins. The tree is annotated with functional characteristics for each MAG (the colored strips represent phylum, the bar charts show completeness in green and contamination in purple, and the gradient heatmap indicates genome size), visualized using iTOL [57]. (**b**) The mean coverage of each MAG after mapping against the read sequence libraries from the Atoud Dam samples; dots represent the mean values, with error bars showing standard deviations. (**c**) Principal component analysis using Pearson correlation coefficients to compute *r* for each dataset (genome size, number of coding genes, coding density, GC content, and contig_N50) versus the control dataset (completeness). *p*-values (* $p \leq 0.0129$) and (**** $p \leq 0.0001$).


**Figure 4.** Antimicrobial profile in the Atoud Dam samples. (**a**) Enrichment analysis of antimicrobial resistance genes. (**b**) Heatmap represents the numerical data of protein domains present in the MAGs for specific mobile genetic elements and virulence factors. All genomes in the bins were initially annotated with RAST-tk to analyze SEED roles for domains in each MAG, with confidence assigned based on a match with the domain family model using an e-value cutoff ($p \leq 0.05$). (**c**) Enrichment analysis of xenobiotic biodegradation. The small chart shows statistical comparisons among different sources of environmental pollutants, categorized into agricultural runoff, industrial pollutants, and polycyclic aromatic hydrocarbons (PAHs), using a nonparametric equivalent of ANOVA on the fraction of the total number of annotated genes and entries for each category (* $p = 0.02$).

Genes (*vanX* and *vanY*) are the key components of vancomycin resistance gene clusters that are harbored by *Enterococcus* bacteria. Although they are typically found at lower abundance than other ARGs in freshwater metagenomic studies, contaminated freshwater bodies that harbor these genes can act as reservoirs for spreading these clinically relevant ARGs [61]. Additionally, cationic antimicrobial peptides have emerged as a promising therapeutic strategy against multidrug-resistant strains such as *Klebsiella pneumoniae* and *Pseudomonas aeruginosa* [62]. Moreover, genes involved in cationic antimicrobial peptide (CAMP) resistance were functionally annotated. The contributions of these genes to CAMP resistance could be through various mechanisms, including efflux pumps (*acrA*, *acrB*, *tolC*, and *cpxR*), modifying the cell envelope (*lpxA*, *eptA*, *phoP*, *arnC*, *arnD*, and *amiABC*), or alterations in protein folding (*dsbA*, *degP*, and *PPIA*) [63,64]. Furthermore, genes such as *mraY*, *mrcA*, and *mrdA*, which are primarily involved in methicillin resistance in *Staphylococcus aureus* via regulating cell wall biosynthesis and penicillin-binding protein functions [65], were also detected in seven MAGs (Figure 4b).

As mentioned, the relative abundance of the primary fecal pollution indicator, *E. coli*, was low (0.073%), indicating that the untreated sewage system was not the main source of ARGs in the Atoud Dam. However, artificial freshwater storage systems always carry a high risk of potential ARG dissemination across species, which may occur through agricultural practices and/or urban runoff [66]. Mobile genetic elements (MGEs), including transposons, integrons, and plasmids, are the key influencing factors that facilitate the propagation of ARGs among bacterial populations in aquatic environments [3]. Within these MGEs, the functional domain profile across the MAG library identified phage capsid proteins, suggesting a possible link between ARGs and phages via transduction [67], as observed in only two MAGs (the *Burkholderiaceae* family (Bin.32) and the *SXOA01* genus (Bin.33)) (Figure 4b). Both bacterial families, *Burkholderiaceae* and *Pirellulaceae* (*SXOA01* genus), are known to exhibit intrinsic resistance to a wide range of common antibiotics [68,69].

Additionally, annotation for integrons, based on the homology of the *IntI* gene sequence, was detected in four families: *Palsa-1439*, *Usitatibacteraceae*, *UBA2999*, and *Burkholderiaceae* (Figure 4b). Integrons are predominantly found in Gram-negative bacteria, occupying nearly 15% of bacterial genomes and encoding *IntI* genes. These genetic elements initially originate in environmental bacteria and play a pivotal role in the dissemination of antibiotic resistance via conjugative transposons and plasmids, facilitating their transfer across species [70]. Furthermore, other mobile genetic elements, such as *Staphylococcal* pathogenicity islands (SaPIs), have been used by *Staphylococcus* and other Gram-positive bacteria to carry virulence genes by exploiting helper phages' life cycles to form phage-like particles, ensuring their spread [71]. Additionally, *Staphylococcal* Phi-Mu50B-like prophages, the dormant form of bacteriophages that are integrated within bacterial chromosomes, provide the necessary viral machinery for encapsidating and transferring SaPIs into new bacterial members, enabling horizontal gene transfer [72]. Genes involved in both (SaPI) and Phi-Mu50B-like prophages were annotated and detected in most of our study (MAGs) library, except the *Kiritimatiellia* class (bin.1) (Figure 4b).

In addition to the role of biotic factors in the proliferation and dissemination of ARGs, abiotic factors act as environmental stressors, triggering selective pressures that further promote resistance [73]. Several xenobiotic degradation pathways were identified for polycyclic aromatic hydrocarbons (naphthalene, toluene, and styrene), pesticides or herbicides (benzoate, atrazine, nitrotoluene, chlorocyclohexane and chlorobenzene, aminobenzoate, ethylbenzene, dioxin, and fluorobenzoate), disinfectants (chloroalkane and chloroalkene), industrial pollutants (caprolactam and xylene), and pharmaceutical and animal waste (steroid). The detection of ~1075 entries annotated for the biodegradation of these environmental pollutants could indicate petroleum spills, industrial wastewater leakage, and, most

significantly, agricultural runoff (Figure 4c). Nearly all MAGs were annotated for resistance against heavy metals, including cobalt, cadmium, and arsenic (Figure 4b). In such environments globally, microbiome dynamics would shift to possess genes capable of degrading or reducing various pollutants (xenobiotics and heavy metals), making freshwater bodies a potential pool of resistome [10].

### *3.5. Metabolic Capacities and Models*

The 30 constructed MAGs from the assembly, with a completeness of over 50% and contamination of less than 10%, were used to reflect the general metabolic and functional capacities of the Atoud Dam's microbial communities. Therefore, the collective translated protein sequences from all MAGs were pooled and used as a query dataset, which was mapped to the KEGG database using the GhostKoala tool. A total of 45,503 entries (~35.4%) were annotated to 328 distinct pathways, mostly belonging to different metabolic pathways, and 6710 KOs were identified (Figure 5a). The high abundance of coding genes was observed to belong to *Verrucomicrobiota*, *Pseudomonadota*, *Planctomycetota*, *Myxococcota*, *Bacteroidota*, *Bdellovibrionota*, *Chloroflexota*, *Acidobacteriota*, *Nitrospirota*, *Gemmatimonadota*, and *Diapherotrites* (*Candidatus* Iainarchaeota) (Figure 5b).

The annotation of merged amino acid sequences across all MAGs revealed complete central carbohydrate metabolic pathways and catabolism. Complete pathways for biosynthesis and energy transfer, including glycolysis, gluconeogenesis, the citric acid cycle (TCA cycle), the pentose phosphate pathway, the glyoxylate cycle, sugar degradation (galacturonate, glucuronate, and galactose), and glycogen storage, were identified. Additionally, complete pathways for peptide and amino acid utilization, phosphoribosyl pyrophosphate biosynthesis for generating nucleotide and amino acid precursors, as well as fatty acid biosynthesis, beta-oxidation, and other lipid metabolism processes, were annotated. A full set of complexes involved in oxidative phosphorylation for ATP production was observed, indicating that respiration and fermentation could be employed. Moreover, all essential machinery for anaerobic respiration, chemolithotrophic respiration, autotrophy (Calvin cycle), anoxygenic phototrophy, and methylotrophy/methanotrophy was also detected, highlighting high metabolic versatility under microaerophilic or anoxic conditions (Table S4).

Distilled and Refined Annotation of Metabolism (DRAM) was used to profile and compare the metabolic potentials of the MAGs (Table S5). Based on DRAM annotations for each MAG bin, the same set of metabolic pathways, particularly metabolic pathways that are involved in the central carbon metabolism and electron transport chain complexes (ETC), were additionally represented, but to a different degree of completeness (Figure 5c). The representations of genes related to the Embden–Meyerhof pathway (glycolysis), pentose phosphate cycle, Entner–Doudoroff pathway, Krebs cycle, glyoxylate cycle, Calvin cycle, Arnon–Buchanan cycle, dicarboxylate–hydroxybutyrate cycle, and Wood–Ljungdahl pathway were found in the bins classified as the *Rubrivivax* genus (Bin.16), *Chitinophagaceae* family (Bin.25), *SXYR01* genus (Bin.27), *Vicinamibacterales* order (Bin.26), *JADYYL01* family (Bin.2), *Pedosphaerales* order (Bin.29), *Planctomycetaceae* family (Bin.7), and *JAHDYP01* genus (Bin.8), suggesting switching between respiration and fermentation or a mixotrophy lifestyle, which was further supported by the DRAM annotations for short-chain fatty acids (SCFAs) and alcohol conversion panel (Figure 6).

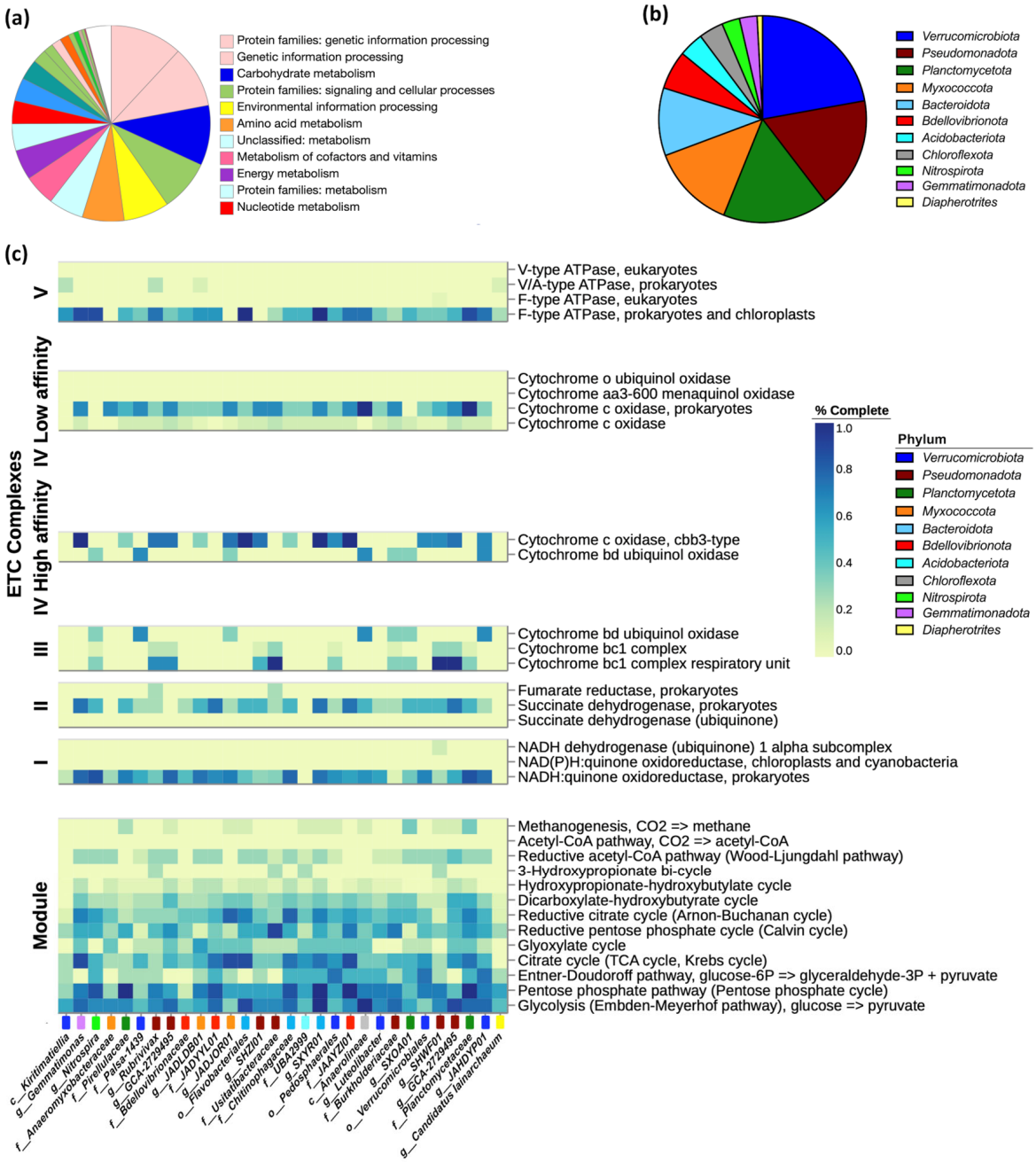


**Figure 5.** Functional assessments of the metabolic pathways of the recovered Atoud Dam MAGs. (**a**) Pie chart representing the general metabolic capacities of all MAGs using a pool of the collectively translated protein sequences as a query dataset. (**b**) Pie chart representing the abundance of coding gene sequences in each phylum representing MAGs. (**c**) Heatmap comparisons of the metabolic profile of each MAG, representing the completeness of relevant central carbon pathways and electron transport chain complexes. The heatmap was generated from DRAM annotations of the predicted coding sequences using the tool's default parameters (minimum contig length of 2500 bp and a bit score threshold of $\geq$60).

As an example of such metabolic flexibility, the *Rubrivivax* genus (Bin.16) is a photosynthetic genus within the class of *Betaproteobacteria*, and its genome (58.48% completeness) was annotated for the presence of fumarate reductase (used under anaerobic conditions) and succinate dehydrogenase (utilized under aerobic conditions). A previous genomic survey identified genes associated with both fumarate reductase and succinate dehydrogenase in this genus, allowing *Rubrivivax* to use different modes of energy production,

such as aerobic and anaerobic respiration, fermentation, and photosynthesis [74]. The same set of annotations and the metabolic flexibility of possessing both fumarate reductase and succinate dehydrogenase, except for the absence of the Entner–Doudoroff pathway, were also represented in Bin.24, but this time to a much greater degree of completeness (72.72% genome completion). The *Usitatibacteraceae* family was isolated from soil and first proposed in 2021. Although previous biochemical and genomic analyses of species members (*Usitatibacter rugosus* and *Usitatibacter palustris*) within the *Usitatibacteraceae* family showed no metabolic pathways for processing inorganic sulfur compounds [75], our assembled genome of the *Usitatibacteraceae* family (Bin.24) was significantly annotated for the presence of genes involved in sulfur metabolism (Figure 6). Having genes for thiosulfate oxidation to sulfate by a complete set of Sox pathway complexes (SoxAX, SoxYZ, SoxB, and SoxCD), thiosulfate reduction to sulfite, and dissimilatory sulfate reduction to sulfide enables this bacterial member to utilize sulfur compounds in a complex cycle. The ability to use sulfate as a terminal electron acceptor to obtain energy anaerobically and oxidize reduced sulfur compounds such as thiosulfate to gain energy aerobically could allow this bacterium to thrive in environments with fluctuating oxygen levels. To our knowledge, this represents the first genomic evidence for both the "forward" and "reverse" dissimilatory sulfate reduction pathways, suggesting the usage of both sulfide and thiosulfate as electron donors in a bacterial member of the *Usitatibacteraceae* family.

A higher level of genome quality (96.11% completeness and 3.01% contamination), but with critically low functional analysis representations in the DRAM annotations, was classified as the only archaeal member, the *Candidatus* Iainarchaeum genus (Bin.9). The limited metabolic capabilities of this archaeal member have been linked to its small genome [76]. The constructed MAG for Bin.9 has a genome size of 968,736 bp (Figure 3a), with a coding density of 0.912 and a contig N50 of 12,067 (Table S2). Previous genomic analysis revealed a lack of a complete TCA cycle and ETCs, along with nutritional auxotrophy for several amino acids and cofactors. This suggests an evolutionary origin from an obligate symbiotic ancestor, albeit with a recent transition to a free-living lifestyle [76]. Another metagenomic analysis study of the DPANN archaea, including the *Diapherotrites* phylum to which the *Candidatus* Iainarchaeum genus belongs, found that the genetic potential identified in DPANN archaea was centered on pyruvate metabolism and fermentation with lactate as an end-product [77]. This was consistent with our findings for the MAG of the *Candidatus* Iainarchaeum genus in the DRAM annotations for the SCFA and alcohol conversion panel (Figure 6). L-lactate dehydrogenase was annotated for its presence in the genome of the *Candidatus* Iainarchaeum genus, despite its rarity in archaea compared to eukaryotes and bacteria [78].

Collectively, our data indicate that pathways related to carbon metabolism, as well as the other functions related to energy production from the recovered MAG pool via community profiling, are carried out in the Atoud Dam by a variety of microbial taxa with diverse metabolism capabilities, thereby reflecting an adaptability to fluctuating oxygen levels and nutrient availability.

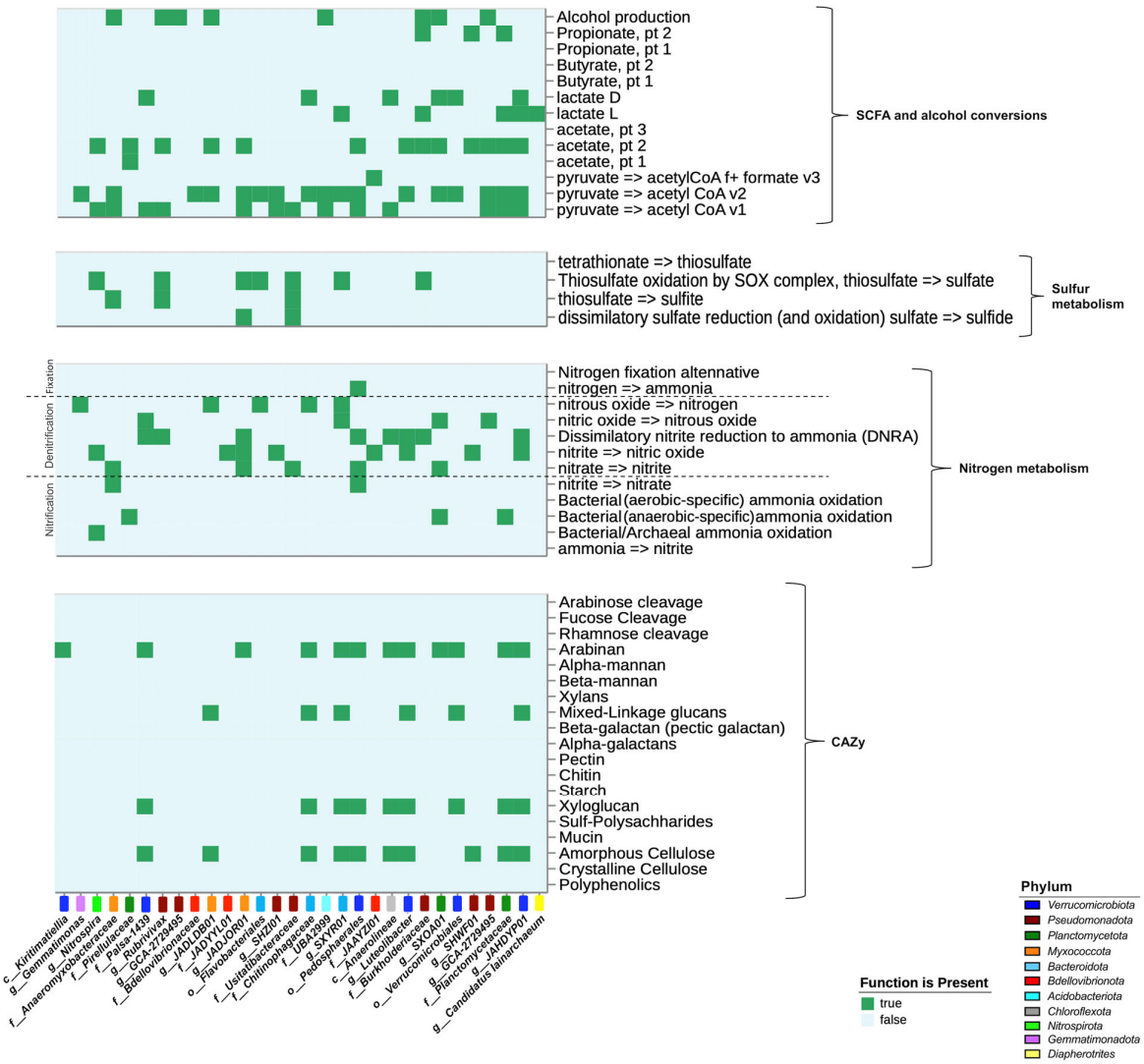


**Figure 6.** Biogeochemical cycling of the recovered Atoud Dam MAGs. Heatmaps generated from DRAM annotations of predicted coding sequences, using the tool's default parameters (minimum contig length of 2500 bp and a bit score threshold of ≥60), show the presence (true) or absence (false) of relevant metabolic functions within each MAG. These functions are based on gene annotation results for carbohydrate-active enzymes (CAZys), nitrogen and sulfur metabolism, and the conversion of short-chain fatty acids (SCFAs) and alcohol.

### *3.6. Biogeochemical Cycles*

In addition to carbon fixation, organic matter degradation is a fundamental process through which microbial communities regulate the carbon cycle. The CAZy panel from the DRAM annotations (Figure 6) exhibited parallel patterns in the presence of carbohydrate-active enzyme (CAZyme) genes in the MAGs, revealing genes related to the cleavage of certain plant cell wall polysaccharides, including only arabinan, mixed-linkage glucan, xyloglucan, and amorphous cellulose. The annotation of these polysaccharides specifically indicates a preference for hydrolyzing more accessible and easily degradable carbohydrates [79]. Consistent with the above-mentioned information, the environmental enrichment in the wetland for microbes that can switch between aerobic and anaerobic respiration and thrive under microaerophilic conditions led to the selective cleavage of these easily accessible polysaccharides. Conversely, hydrolyzing the highly structured crystalline cellulose or lignin, which is an energy-consuming and slower process, is not ideal in such low-oxygen wetland ecosystems [80].

The overrepresentation of glycoside hydrolases (GHs), at ~32 genes, was found in all 6 bacterial members of the *Verrucomicrobiota* phylum, even in its hardly cultivable, rarely detected, and poorly annotated *Kiritimatiellia* class (Bin.1) [81]. More GH genes were also recovered in other phyla, including *Bacteroidota* (18 genes), *Planctomycetota* (5 genes), *Myxococcota* (5 genes), *Chloroflexota* (4 genes), and *Pseudomonadota* (1 gene). Although aquatic polysaccharide degraders can differ significantly depending on the type of substrates, nutrient concentrations, and oxygen availability [82], consistent with a previous study, the *Verrucomicrobiota* phylum has been recognized for its significant environmental role in degrading plant-derived organic matter [83]. A previous genomic analysis study observed abundant arrays of GH genes across 19 freshwater *Verrucomicrobiota* MAGs, representing 78 different GH families, metabolizing diverse polysaccharides, with notable GH coding density reaching up to 4.9% in some of these MAGs. This is evidently attributed to the ability of this phylum to utilize a wide range of sugar polymers, the key components of the plant biomass [84].

Despite the consistent functional analysis of the CAZyme genes in a freshwater ecosystem, it remains unclear whether the annotations merely reflect early decomposition stages due to the limited sampling approaches, such as collecting samples during different seasons with broader spatial coverage. However, nitrogen metabolism could serve as an indicator of decomposition rate, as it is inversely affected by the initial carbon-to-nitrogen ratio. In other words, high nitrogen levels can lead to a higher decomposition rate because microbes in these conditions have the required nitrogen for amino acid synthesis and growth [82]. Although nitrogen availability is vital for primary producers, anthropogenic activities, such as excessive fertilizer use, can disrupt the nitrogen cycle, leading to greenhouse gas emissions (e.g., nitrous oxide) and eutrophication [85]. The nitrogen metabolism panel from the DRAM annotations (Figure 6) revealed genes involved in a complete nitrogen cycle, starting with the fixation of inert nitrogen gas. The cycle then continually transforms nitrogen from the most reduced form, ammonia, to the most oxidized form, nitrate, and back to inert nitrogen gas, indicating broad contributions from a diverse microbial community.

Nitrogenase genes (*nifD*, *nifH*, and *nifK*), which are involved in the nitrogen fixation process, converting atmospheric nitrogen ($N_2$) into ammonia ($NH_3$), were found in only one MAG classified as belonging to the *Pedosphaerales* order (Bin.29) within the *Verrucomicrobiota* phylum. The presence of *nifD* (which encodes the nitrogenase molybdenum-iron protein α-chain), *nifH* (which encodes the nitrogenase iron protein), and *nifK* (the β-chain of nitrogenase) suggests that this bacterium could be diazotrophic. Considering the rarity of *Verrucomicrobiota* members acting as nitrogen fixers, likely due to research limitations, *Pedosphaerales* is also recognized as a poorly studied order. *Pedosphaerales* have been shown to be abundant in soil bacterial communities in tallgrass prairies in North America [86]. Consistently, another study identified *Pedosphaerales*, along with the bacterial orders *Planctomycetales* and *Syntrophobacterales*, as indicator taxa in large soil macroaggregates. Since both *Planctomycetales* and *Syntrophobacterales* include anaerobic bacteria, this study suggests that these macroaggregates may harbor anaerobic zones [87], which provide the necessary conditions for oxygen-sensitive processes such as nitrogen fixation. These habitats—large macroaggregates of soil—have previously been evaluated for their higher nitrogen-cycling enzyme activity [88]. Additionally, a recent study detected a high abundance of *Pedosphaerales* lineages in soil microbial communities, along with nitrogen cycle-related gene expressions throughout different stages of the growing season, though the study did not link these gene expressions to specific microbes [89]. To our knowledge, no experimental evidence or genomic survey has documented the potential for nitrogen fixation in the *Pedosphaerales* order.

In addition to converting inert nitrogen into the key intermediate, ammonia, a series of nitrogen-transforming processes was detected based on oxygen levels. The hydroxylamine oxidoreductase (*hao*) gene, involved in anaerobic ammonium oxidation (anammox), was recovered. Anammox typically occurs in anoxic environments, such as wetlands, and is responsible for 50% of the removal of fixed N back into inert N in nature. The presence of this gene was detected in MAGs that were classified as both *Planctomycetaceae* (Bin.7) and *Pirellulaceae* (Bin.14) families, as well as the *SXOA01* genus (Bin.33). These anammox bacteria, all found within the *Planctomycetota* phylum, have been preferably selected as environmentally friendlier (negligible $N_2O$ emissions) and more cost-effective than denitrifiers for wastewater treatment due to their lower oxygen requirements and carbon-free cultivation [90]. Anammox bacteria normally inhabit niches where both reduced (ammonia) and oxidized (nitrite) forms are simultaneously present. At the aerobic–anaerobic interface in aquatic ecosystems, including sediment–water interfaces, the anaerobic degradation of organic matter produces ammonia, while nitrite can be produced via aerobic ammonia oxidation [91].

Aerobic ammonia oxidation was represented by another key MAG player in the N cycle, classified as the *Nitrospira* genus (Bin.12) and known as comammox for its complete ammonia-oxidizing performance under aerobic conditions [92]. The DRAM annotations detected the *pmoA-amoA* and *pmoB-amoB* genes, which encode the ammonia monooxygenase (AMO) complex that initiates the oxidation of ammonia ($NH_3$) to hydroxylamine ($NH_2OH$). Additionally, genes for denitrification (including *nirD* and *nirK*) were detected, which are involved in reducing nitrate to nitric oxide. This allows *Nitrospira* to use nitrate as an electron acceptor when oxygen is limited, highlighting the metabolic versatility of this genus as microaerophilic [93]. More nitrification genes, *nxrA* and *nxrB* (nitrite oxidoreductase a and b subunits, respectively), were detected in the MAGs that were classified as the *Pedosphaerales* order (Bin.29) and *Anaeromyxobacteraceae* family (Bin.13).

Genes involved in denitrification, a facultative anaerobic respiratory process that converts nitrate into nitrogen gas, were recovered from several MAGs. These genes included those encoding the membrane-bound nitrate reductase complex (*narG*, *narH*, and *narI*) and periplasmic nitrate reductase (*napA* and *napB*), both of which catalyze the reduction of nitrate to nitrite. In addition, genes encoding nitrite reductase (*nirK* and *nirS*), responsible for the reduction of nitrite to nitric oxide, as well as nitric oxide reductase (*norB* and *norC*), which catalyze the reduction of nitric oxide to nitrous oxide, were also detected. Additionally, the presence of *nosZ*, which encodes nitrous oxide reductase, suggests the potential for further reduction of nitrous oxide to nitrogen gas. Eliminating nitrate through denitrification can produce nitrous oxide ($N_2O$), a potent greenhouse gas and a major ozone-depleting substance, as an intermediate [94].

In contrast, dissimilatory nitrate reduction to ammonia (DNRA) is a pathway that recycles nitrogen within an ecosystem, favoring high organic carbon levels relative to nitrate, and occurs in oxygen-limited environments, such as wetlands [95]. Primary marker genes *nrfA* (encodes cytochrome c nitrite reductase a subunit) and *nrfH* (encodes cytochrome c nitrite reductase small subunit) were recovered from several MAGs that were classified as the *Palsa-1439* family (Bin.15), *Rubrivivax* genus (Bin.16), *JADJOR01* genus (Bin.20), *Pedosphaerales* order (Bin.29), *Anaerolineae* class (Bin.30), *Luteolibacter* genus (Bin.31), *Burkholderiaceae* family (Bin.32), and *JAHDYP01* genus (Bin.8). Bacterial members of the *Verrucomicrobiota* phylum, including *Verrucomicrobiae* [96] and *Luteolibacter* [97], have been reported to have the genomic potential to perform DNRA based on gene contents. In addition, a previous metagenomic study investigating *Chloroflexota* phylum diversity in bioreactors identified *Anaerolineae* bacteria under anaerobic conditions that participate in nitrogen removal via nitrate/nitrite reduction genes, suggesting DNRA potential [98]. A previous

study on the genus *Rubrivivax* showed that nitrite reduction can be metabolically linked to photosynthetic reactions via a specific *c*-type cytochrome, using nitrite as an electron acceptor under anoxic conditions, suggesting the potential for the DNRA pathway [99]. *Burkholderiaceae*, which was recently identified in contaminated paddy, has been reported to possess the *nrfA* gene [100]. *JADJOR01*, a genus of uncultivated bacteria within the *Myxococcota* phylum, has previously had its genome recovered from the MAGs of wastewater treatment plants. Interestingly, the genomic investigation showed that *JADJOR01*, unlike other *Myxococcota* members, lacks the complex social behaviors of aggregation and fruiting body formation, which are unnecessary survival machineries in a nutrient-rich activated sludge environment. Additionally, the *JADJOR01* genus was proposed as an anaerobe, relying on fermentation, nitrate reduction, or sulfate reduction to generate energy, along with the possession of specific glycoside hydrolases (GH13), allowing it to degrade the cell walls of other bacteria [101]. This aligns with our findings regarding the metabolic profile of this lineage, as indicated in the DRAM annotations.

All in all, based on the DRAM N metabolism panel of our data, it is noticeable that the denitrification annotation profile was more enriched than the conversion of ammonia to nitrate (nitrification) in terms of the abundance of the annotated genes and the number of involved MAGs, suggesting active nitrogen removal from the ecosystem under anoxic or suboxic environmental conditions. Besides the significant annotations of xenobiotic degradation pathways and the relatively high abundance of *Microcystis aeruginosa* (4.52%) as the species with the highest assigned reads, this could signify the possibility of eutrophication (high nutrient loading), which sets an ideal condition for algal blooms, thereby leading to oxygen depletion [102,103].

Under such eutrophic conditions, nitrogen metabolism interacts cooperatively with sulfur metabolism, particularly the reduction of nitrogen through denitrification and sulfur oxidation via SOX systems [104]. Consistent with these previous findings, our DRAM S metabolism panel also exhibited this enriched correlation between sulfur oxidation and nitrogen reduction. As mentioned earlier, the MAG *Usitatibacteraceae* family (Bin.24) possesses a complete set of genes (*soxXYZABCD*) for thiosulfate oxidation to sulfate via the Sox enzyme system. Additionally, another complete thiosulfate oxidation pathway was identified in the MAG *Rubrivivax* genus (Bin.16), aligning with previous genomic studies [105] and showing the potential to grow using thiosulfate as an inorganic electron donor, oxidizing it to sulfate [106]. Other MAGs, such as the *Burkholderiaceae* family (Bin.32), *SXYR01* genus (Bin.27), *Flavobacteriales* order (Bin.22), *JADJOR01* genus (Bin.20), and *Nitrospira* genus (Bin.12), exhibited incomplete Sox complexes (lacking SoxCD), suggesting partial oxidation of thiosulfate that could lead to the accumulation of elemental sulfur ($S^0$). Under microaerobic or anoxic conditions, this intermediate could increase the risk of forming toxic hydrogen sulfide gas ($H_2S$) [107].

## 4. Conclusions

This study provides the first comprehensive insights into the microbial composition, abundances, and functional attributes in Atoud Dam's freshwater system, indicating early signs of ecological disturbance. Shotgun metagenomic analyses uncovered a diverse community across all microbial groups, with habitable features of an aquatic freshwater microbiome. The assignment of 4.52% of all sequence reads at the species level to the cyanobacterium (*Microcystis aeruginosa*) points to a possible eutrophication process with a potential risk of future algal blooms. The co-assembled contigs generated 30 MAGs that represent 11 diverse prokaryotic phyla, paving the way for potentially novel genomes. Based on genomic content and functional annotations, some of these MAGs show putatively novel metabolic potentials. For instance, the archaeal genus *Candidatus* Iainarchaeum,

annotated as a fermenter, produces lactate as an end product. Additionally, our study highlights previously unreported novel pathways for nitrogen fixation and thiosulfate oxidation involving the candidate lineages *Pedosphaerales* and *Usitatibacteraceae*, respectively.

The functional analysis of all MAGs coding sequences shows that the microbial community residing in the Atoud Dam harbors a significant number of antibiotic resistance genes, mainly β-lactam resistance genes. In addition, detecting mobile genetic elements using protein domain profiles for each MAG sheds light on the contributions of these elements to the spread of ARGs that pose health hazards. The eutrophication process is further evidenced by the functional analysis of nitrogen and sulfur metabolism. The DRAM annotation revealed increased activity in denitrification and sulfur oxidation, likely due to nutrient accumulation from agricultural practices, as indicated by the significantly enriched xenobiotic biodegradation pathways. Although the study's results provide fundamental data on local microbial diversity for the first time and unravel putative novel metabolic functions, they are limited by the seasonal and spatial sampling, which restricts broader conclusions about eutrophication status. Future studies should incorporate sampling across seasons with longitudinal monitoring and include a broader range of water bodies from across Asir Province for comparative analysis. The inclusion of these steps would provide a better understanding of ecosystem-level impacts on microbial communities in light of climate change and land-use changes.

**Supplementary Materials:** The following supporting information can be downloaded at: https://www.mdpi.com/article/10.3390/d18010016/s1. Figure S1: Sampling Diagram; File S1: Krona_AtoudDam_MicrobialGroups.html; Table S1: Taxon_Details.xlsx; Table S2: GTDB-Tk_Classifications.xlsx; Table S3: ARGs; Table S4: Metabolic_Capacities.xlsx; Table S5: metabolism_summary(DRAM).xlsx.

**Funding:** This research was funded by Deanship of Research and Graduate Studies at King Khalid University, the KSA (grant number: RGP.1/42/46).

**Institutional Review Board Statement:** Not applicable.

**Data Availability Statement:** Sequence reads were deposited in the National Center for Biotechnology Information (accession number: PRJNA1372091). Further inquiries can be directed to the corresponding author.

**Acknowledgments:** The author extends their appreciation to the Deanship of Research and Graduate Studies at King Khalid University, the KSA, for funding this work through the Small Research Group (grant number: RGP.1/42/46).

**Conflicts of Interest:** The author declares no conflicts of interest.

## References

1. Gao, W.P.; Zhang, H.; Wang, X.; Yang, X.; An, C. From water to sediment: A meta-analysis of microplastic distribution and the impact of dams in reservoir ecosystems. *Eco-Environ. Health* **2025**, *4*, 100188. [CrossRef] [PubMed]
2. Grossart, H.P.; Massana, R.; McMahon, K.D.; Walsh, D.A. Linking metagenomics to aquatic microbial ecology and biogeochemical cycles. *Limnol. Oceanogr.* **2019**, *65*, S2–S20. [CrossRef]
3. Behera, B.K.; Dehury, B.; Rout, A.K.; Patra, B.; Mantri, N.; Chakraborty, H.J.; Sarkar, D.J.; Kaushik, N.K.; Bansal, V.; Singh, I.; et al. Metagenomics study in aquatic resource management: Recent trends, applied methodologies and future needs. *Gene Rep.* **2021**, *25*, 101372. [CrossRef]
4. Downing, J.A.; Prairie, Y.T.; Cole, J.J.; Duarte, C.M.; Tranvik, L.J.; Striegl, R.G.; McDowell, W.H.; Kortelainen, P.; Caraco, N.F.; Melack, J.M.; et al. The global abundance and size distribution of lakes, ponds, and impoundments. *Limnol. Oceanogr.* **2006**, *51*, 2388–2397. [CrossRef]
5. Song, H.; Li, Z.; Du, B.; Wang, G.; Ding, Y. Bacterial communities in sediments of the shallow Lake Dongping in China. *J. Appl. Microbiol.* **2012**, *112*, 79–89. [CrossRef]

6. Gougoulias, C.; Clark, J.M.; Shaw, L.J. The role of soil microbes in the global carbon cycle: Tracking the below-ground microbial processing of plant-derived carbon for manipulating carbon dynamics in agricultural systems. *J. Sci. Food Agric.* **2014**, *94*, 2362–2371. [CrossRef]
7. Kuypers, M.M.M.; Marchant, H.K.; Kartal, B. The microbial nitrogen-cycling network. *Nat. Rev. Microbiol.* **2018**, *16*, 263–276. [CrossRef]
8. Bowles, M.W.; Mogollón, J.M.; Kasten, S.; Zabel, M.; Hinrichs, K.U. Global rates of marine sulfate reduction and implications for sub-sea-floor metabolic activities. *Science* **2014**, *344*, 889–891. [CrossRef]
9. Ma, L.-C.; Zhao, H.-Q.; Wu, L.B.; Cheng, Z.-L.; Liu, C. Impact of the microbiome on human, animal, and environmental health from a One Health perspective. *Sci. One Health* **2023**, *2*, 100037. [CrossRef]
10. Mittal, P.; Prasoodanan, P.V.; Dhakan, D.B.; Kumar, S.; Sharma, V.K. Metagenome of a polluted river reveals a reservoir of metabolic and antibiotic resistance genes. *Environ. Microbiome* **2019**, *14*, 5. [CrossRef]
11. Berry, T.E.; Saunders, B.J.; Coghlan, M.L.; Stat, M.; Jarman, S.; Richardson, A.J.; Davies, C.H.; Berry, O.; Harvey, E.S.; Bunce, M. Marine environmental DNA biomonitoring reveals seasonal patterns in biodiversity and identifies ecosystem responses to anomalous climatic events. *PLoS Genet.* **2019**, *15*, e1007943. [CrossRef] [PubMed]
12. Sereika, M.; Mussig, A.J.; Jiang, C.; Knudsen, K.S.; Jensen, T.B.N.; Petriglieri, F.; Yang, Y.; Jørgensen, V.R.; Delogu, F.; Sørensen, E.A.; et al. Genome-resolved long-read sequencing expands known microbial diversity across terrestrial habitats. *Nat. Microbiol.* **2025**, *10*, 2018–2030. [CrossRef]
13. Balasubramanian, V.K.; Joseph Maran, M.I.; Ramteke, D.; Vijaykumar, D.S.; Kottarathail Rajendran, A.; Ramachandran, P.; Ramachandran, R. Environmental DNA reveals aquatic biodiversity of an urban backwater area, southeast coast of India. *Mar. Pollut. Bull.* **2021**, *171*, 112786. [CrossRef]
14. Gao, Y.; Luo, H.; Lyu, H.; Yang, H.; Yousuf, S.; Huang, S.; Liu, Y.X. Benchmarking short-read metagenomics tools for removing host contamination. *Gigascience* **2025**, *14*, giaf004. [CrossRef] [PubMed]
15. Martin, M. Cutadapt removes adapter sequences from high-throughput sequencing reads. *EMBnet* **2011**, *17*, 3. [CrossRef]
16. de Sena Brandine, G.; Smith, A.D. Falco: High-speed FastQC emulation for quality control of sequencing data. *F1000Research* **2019**, *8*, 1874. [CrossRef]
17. Lu, J.; Rincon, N.; Wood, D.E.; Breitwieser, F.P.; Pockrandt, C.; Langmead, B.; Salzberg, S.L.; Steinegger, M. Author Correction: Metagenome analysis using the Kraken software suite. *Nat. Protoc.* **2024**, *17*, 2815–2839. [CrossRef]
18. Lu, J.; Breitwieser, F.P.; Thielen, P.; Salzberg, S.L. Bracken: Estimating species abundance in metagenomics data. *PeerJ Comput. Sci.* **2017**, *3*, e104. [CrossRef]
19. Li, D.; Luo, R.; Liu, C.M.; Leung, C.M.; Ting, H.F.; Sadakane, K.; Yamashita, H.; Lam, T.W. MEGAHIT v1.0: A fast and scalable metagenome assembler driven by advanced methodologies and community practices. *Methods* **2016**, *102*, 3–11. [CrossRef]
20. Mikheenko, A.; Saveliev, V.; Gurevich, A. MetaQUAST: Evaluation of metagenome assemblies. *Bioinformatics* **2016**, *32*, 1088–1090. [CrossRef]
21. Uritskiy, G.V.; DiRuggiero, J.; Taylor, J. MetaWRAP-a flexible pipeline for genome-resolved metagenomic data analysis. *Microbiome* **2018**, *6*, 158. [CrossRef] [PubMed]
22. Olm, M.R.; Brown, C.T.; Brooks, B.; Banfield, J.F. dRep: A tool for fast and accurate genomic comparisons that enables improved genome recovery from metagenomes through de-replication. *ISME J.* **2017**, *11*, 2864–2868. [CrossRef] [PubMed]
23. Chklovski, A.; Parks, D.H.; Woodcroft, B.J.; Tyson, G.W. CheckM2: A rapid, scalable and accurate tool for assessing microbial genome quality using machine learning. *Nat. Methods* **2023**, *20*, 1203–1212. [CrossRef] [PubMed]
24. Kim, D.; Langmead, B.; Salzberg, S.L. HISAT: A fast spliced aligner with low memory requirements. *Nat. Methods* **2015**, *12*, 357–360. [CrossRef]
25. Chaumeil, P.A.; Mussig, A.J.; Hugenholtz, P.; Parks, D.H. GTDB-Tk v2: Memory friendly classification with the genome taxonomy database. *Bioinformatics* **2022**, *38*, 5315–5316. [CrossRef]
26. Price, M.N.; Dehal, P.S.; Arkin, A.P. FastTree 2--approximately maximum-likelihood trees for large alignments. *PLoS ONE* **2010**, *5*, e9490. [CrossRef]
27. Brettin, T.; Davis, J.J.; Disz, T.; Edwards, R.A.; Gerdes, S.; Olsen, G.J.; Olson, R.; Overbeek, R.; Parrello, B.; Pusch, G.D.; et al. RASTtk: A modular and extensible implementation of the RAST algorithm for building custom annotation pipelines and annotating batches of genomes. *Sci. Rep.* **2015**, *5*, 8365. [CrossRef]
28. Kanehisa, M.; Sato, Y.; Morishima, K. BlastKOALA and GhostKOALA: KEGG Tools for Functional Characterization of Genome and Metagenome Sequences. *J. Mol. Biol.* **2016**, *428*, 726–731. [CrossRef]
29. Shaffer, M.; Borton, M.A.; McGivern, B.B.; Zayed, A.A.; La Rosa, S.L.; Solden, L.M.; Liu, P.; Narrowe, A.B.; Rodriguez-Ramos, J.; Bolduc, B.; et al. DRAM for distilling microbial metabolism to automate the curation of microbiome function. *Nucleic Acids Res.* **2020**, *48*, 8883–8900. [CrossRef]
30. McMurdie, P.J.; Holmes, S. phyloseq: An R package for reproducible interactive analysis and graphics of microbiome census data. *PLoS ONE* **2013**, *8*, e61217. [CrossRef]

31. Ondov, B.D.; Bergman, N.H.; Phillippy, A.M. Interactive metagenomic visualization in a Web browser. *BMC Bioinform.* **2011**, *12*, 385. [CrossRef]
32. Brar, B.; Kumar, R.; Sharma, D.; Sharma, A.K.; Thakur, K.; Mahajan, D. Metagenomic analysis reveals diverse microbial community and potential functional roles in Baner rivulet, India. *J. Genet. Eng. Biotechnol.* **2023**, *21*, 147. [CrossRef]
33. Zhang, Q.; Wu, Z.; Zhao, J.; Wang, G.; Hao, J.; Wang, S.; Lin, Y.; Guan, H.; Zhang, J.; Jian, S.; et al. Composition and Functional Characteristics and Influencing Factors of Bacterioplankton Community in the Huangshui River, China. *Microorganisms* **2021**, *9*, 2260. [CrossRef] [PubMed]
34. Fontaine, L.; Pin, L.; Savio, D.; Friberg, N.; Kirschner, A.K.T.; Farnleitner, A.H.; Eiler, A. Bacterial bioindicators enable biological status classification along the continental Danube river. *Commun. Biol.* **2023**, *6*, 862. [CrossRef] [PubMed]
35. Hu, F.; Wang, P.; Li, Y.; Ling, J.; Ruan, Y.; Yu, J.; Zhang, L. Bioremediation of environmental organic pollutants by *Pseudomonas aeruginosa*: Mechanisms, methods and challenges. *Environ. Res.* **2023**, *239*, 117211. [CrossRef] [PubMed]
36. Satola, B.; Wübbeler, J.H.; Steinbüchel, A. Metabolic characteristics of the species Variovorax paradoxus. *Appl. Microbiol. Biotechnol.* **2013**, *97*, 541–560. [CrossRef] [PubMed]
37. Gan, H.M.; Lee, Y.P.; Austin, C.M. Nanopore Long-Read Guided Complete Genome Assembly of Hydrogenophaga intermedia, and Genomic Insights into 4-Aminobenzenesulfonate, p-Aminobenzoic Acid and Hydrogen Metabolism in the Genus Hydrogenophaga. *Front. Microbiol.* **2017**, *8*, 1880. [CrossRef]
38. Kolvenbach, B.A.; Corvini, P.F. The degradation of alkylphenols by *Sphingomonas* sp. strain TTNP3—A review on seven years of research. *N. Biotechnol.* **2012**, *30*, 88–95. [CrossRef]
39. Avontuur, J.R.; Wilken, P.M.; Palmer, M.; Coetzee, M.P.A.; Stępkowski, T.; Venter, S.N.; Steenkamp, E.T. Complex evolutionary history of photosynthesis in *Bradyrhizobium*. *Microb. Genom.* **2023**, *9*, 001105. [CrossRef]
40. Ju, J.H.; Kim, J.S.; Lee, D.H.; Jeon, J.H.; Heo, S.Y.; Seo, J.W.; Kim, C.H.; Park, D.S.; Oh, B.R. *Thermomonas aquatica* sp. nov., isolated from an industrial wastewater treatment plant. *Int. J. Syst. Evol. Microbiol.* **2019**, *69*, 3399–3404. [CrossRef]
41. Bairagi, N.; Keffer, J.L.; Heydt, J.C.; Maresca, J.A. Genome editing in ubiquitous freshwater Actinobacteria. *Appl. Environ. Microbiol.* **2024**, *90*, e00865-24. [CrossRef] [PubMed]
42. Lorková, Z.; Cimermanová, M.; Piknová, M.; Adhvaryu, S.; Pristaš, P.; Kisková, J. Environmental impact on the genome shaping of putative new Streptomyces species. *BMC Microbiol.* **2025**, *25*, 72. [CrossRef] [PubMed]
43. Zhu, J.; Liu, R.; Cao, N.; Yu, J.; Liu, X.; Yu, Z. Mycobacterial metabolic characteristics in a water meter biofilm revealed by metagenomics and metatranscriptomics. *Water Res.* **2019**, *153*, 315–323. [CrossRef] [PubMed]
44. Onley, J.R.; Ahsan, S.; Sanford, R.A.; Löffler, F.E. Denitrification by Anaeromyxobacter dehalogenans, a Common Soil Bacterium Lacking the Nitrite Reductase Genes nirS and nirK. *Appl. Environ. Microbiol.* **2018**, *84*, e01985-17. [CrossRef]
45. Thomas, S.H.; Padilla-Crespo, E.; Jardine, P.M.; Sanford, R.A.; Löffler, F.E. Diversity and distribution of anaeromyxobacter strains in a uranium-contaminated subsurface environment with a nonuniform groundwater flow. *Appl. Environ. Microbiol.* **2009**, *75*, 3679–3687. [CrossRef]
46. Wynne, T.T.; Stumpf, R.P.; Tomlinson, M.C.; Dyble, J. Characterizing a cyanobacterial bloom in western Lake Erie using satellite imagery and meteorological data. *Limnol. Oceanogr.* **2010**, *55*, 2025–2036. [CrossRef]
47. Rosen, B.H.; Davis, T.W.; Gobler, C.J.; Kramer, B.J.; Loftin, K.A. *Cyanobacteria of the 2016 Lake Okeechobee and Okeechobee Waterway Harmful Algal Bloom*; 2331-1258; US Geological Survey: Reston, VA, USA, 2017.
48. Preece, E.P.; Hardy, F.J.; Moore, B.C.; Bryan, M. A review of microcystin detections in Estuarine and Marine waters: Environmental implications and human health risk. *Harmful Algae* **2017**, *61*, 31–45. [CrossRef]
49. Cook, K.V.; Li, C.; Cai, H.; Krumholz, L.R.; Hambright, K.D.; Paerl, H.W.; Steffen, M.M.; Wilson, A.E.; Burford, M.A.; Grossart, H.P.; et al. The global Microcystis interactome. *Limnol. Oceanogr.* **2020**, *65*, S194–S207. [CrossRef]
50. Chen, J.; Zhang, T.; Sun, L.; Liu, Y.; Li, D.; Leng, X.; An, S. Abundance trade-offs and dominant taxa maintain the stability of the bacterioplankton community underlying Microcystis blooms. *Front. Microbiol.* **2023**, *14*, 1181341. [CrossRef]
51. Yamamoto, K.; Yoneda, Y.; Makino, A.; Tanaka, Y.; Meng, X.-Y.; Hashimoto, J.; Shin-ya, K.; Satoh, N.; Fujie, M.; Toyama, T.; et al. Complete Genome Sequence of Luteitalea sp. Strain TBR-22. *Microbiol. Resour. Announc.* **2022**, *11*, e00455-21. [CrossRef]
52. Xue, Q.; Zuo, Z.; Zhou, H.; Zhou, J.; Zhang, S.; Han, J.; Zhao, D.; Xiang, H. *Salinadaptatus halalkaliphilus* gen. nov., sp. nov., a haloalkaliphilic archaeon isolated from salt pond in Inner Mongolia Autonomous Region, China. *Int. J. Syst. Evol. Microbiol.* **2021**, *71*, 004584. [CrossRef] [PubMed]
53. Ferrelli, M.L.; Salvador, R. Effects of Mixed Baculovirus Infections in Biological Control: A Comprehensive Historical and Technical Analysis. *Viruses* **2023**, *15*, 1838. [CrossRef] [PubMed]
54. Breitwieser, F.P.; Salzberg, S.L. Pavian: Interactive analysis of metagenomics data for microbiome studies and pathogen identification. *Bioinformatics* **2020**, *36*, 1303–1304. [CrossRef] [PubMed]
55. Reichenberger, E.R.; Rosen, G.; Hershberg, U.; Hershberg, R. Prokaryotic nucleotide composition is shaped by both phylogeny and the environment. *Genome Biol. Evol.* **2015**, *7*, 1380–1389. [CrossRef]

56. Zhang, L.; Fang, X.; Liao, H.; Zhang, Z.; Zhou, X.; Han, L.; Chen, Y.; Qiu, Q.; Li, S.C. A comprehensive investigation of metagenome assembly by linked-read sequencing. *Microbiome* **2020**, *8*, 156. [CrossRef]
57. Letunic, I.; Bork, P. Interactive Tree of Life (iTOL) v6: Recent updates to the phylogenetic tree display and annotation tool. *Nucleic Acids Res.* **2024**, *52*, W78–W82. [CrossRef]
58. Wand, M.E.; Darby, E.M.; Blair, J.M.A.; Sutton, J.M. Contribution of the efflux pump AcrAB-TolC to the tolerance of chlorhexidine and other biocides in *Klebsiella* spp. *J. Med. Microbiol.* **2022**, *71*, 001496. [CrossRef]
59. Hussain, H.I.; Aqib, A.I.; Seleem, M.N.; Shabbir, M.A.; Hao, H.; Iqbal, Z.; Kulyar, M.F.; Zaheer, T.; Li, K. Genetic basis of molecular mechanisms in beta-lactam resistant gram-negative bacteria. *Microb. Pathog.* **2021**, *158*, 105040. [CrossRef]
60. Navarro, A.; Sanseverino, I.; Cappelli, F.; Lahm, A.; Niegowska, M.; Fabbri, M.; Paracchini, V.; Petrillo, M.; Skejo, H.; Valsecchi, S.; et al. Study of antibiotic resistance in freshwater ecosystems with low anthropogenic impact. *Sci. Total Environ.* **2023**, *857*, 159378. [CrossRef]
61. Guo, X.; Zhang, X.; Ni, N.; Shi, M.; Wang, N. Fate and Proliferation of Vancomycin Resistance Genes in Two Typical Pharmaceutical Wastewater Treatment Plants. *Water* **2024**, *16*, 114. [CrossRef]
62. Rivera-Sánchez, S.P.; Agudelo-Góngora, H.A.; Oñate-Garzón, J.; Flórez-Elvira, L.J.; Correa, A.; Londoño, P.A.; Londoño-Mosquera, J.D.; Aragón-Muriel, A.; Polo-Cerón, D.; Ocampo-Ibáñez, I.D. Antibacterial Activity of a Cationic Antimicrobial Peptide against Multidrug-Resistant Gram-Negative Clinical Isolates and Their Potential Molecular Targets. *Molecules* **2020**, *25*, 5035. [CrossRef]
63. Cole, J.N.; Nizet, V. Bacterial Evasion of Host Antimicrobial Peptide Defenses. *Microbiol. Spectr.* **2016**, *4*, 413–443. [CrossRef] [PubMed]
64. Weatherspoon-Griffin, N.; Yang, D.; Kong, W.; Hua, Z.; Shi, Y. The CpxR/CpxA two-component regulatory system up-regulates the multidrug resistance cascade to facilitate Escherichia coli resistance to a model antimicrobial peptide. *J. Biol. Chem.* **2014**, *289*, 32571–32582. [CrossRef]
65. Lade, H.; Kim, J.S. Molecular Determinants of beta-Lactam Resistance in Methicillin-Resistant Staphylococcus aureus (MRSA): An Updated Review. *Antibiotics* **2023**, *12*, 1362. [CrossRef] [PubMed]
66. Guo, Z.F.; Boeing, W.J.; Xu, Y.Y.; Borgomeo, E.; Liu, D.; Zhu, Y.G. Data-driven discoveries on widespread contamination of freshwater reservoirs by dominant antibiotic resistance genes. *Water Res.* **2023**, *229*, 119466. [CrossRef] [PubMed]
67. Blanco-Picazo, P.; Morales-Cortes, S.; Ramos-Barbero, M.D.; Garcia-Aljaro, C.; Rodriguez-Rubio, L.; Muniesa, M. Dominance of phage particles carrying antibiotic resistance genes in the viromes of retail food sources. *ISME J.* **2023**, *17*, 195–203. [CrossRef]
68. Wang, B.; Zhang, J.; Chen, L.; Ijaz, M.; Bi, J.; Li, C.; Dong, D.; Wang, Y.; Li, B.; Luo, J.; et al. Burkholderia Phages and Control of Burkholderia-Associated Human, Animal, and Plant Diseases. *Microorganisms* **2025**, *13*, 1873. [CrossRef]
69. Guedes, B.; Godinho, O.; Quinteira, S.; Lage, O.M. Antimicrobial Resistance Profile of Planctomycetota Isolated from Oyster Shell Biofilm: Ecological Relevance within the One Health Concept. *Appl. Microbiol.* **2024**, *4*, 16–26. [CrossRef]
70. Ali, N.; Ali, I.; Din, A.U.; Akhtar, K.; He, B.; Wen, R. Integrons in the Age of Antibiotic Resistance: Evolution, Mechanisms, and Environmental Implications: A Review. *Microorganisms* **2024**, *12*, 2579. [CrossRef]
71. Ram, G.; Chen, J.; Kumar, K.; Ross, H.F.; Ubeda, C.; Damle, P.K.; Lane, K.D.; Penadés, J.R.; Christie, G.E.; Novick, R.P. Staphylococcal pathogenicity island interference with helper phage reproduction is a paradigm of molecular parasitism. *Proc. Natl. Acad. Sci. USA* **2012**, *109*, 16300–16305. [CrossRef]
72. Ingmer, H.; Gerlach, D.; Wolz, C. Temperate Phages of Staphylococcus aureus. *Microbiol. Spectr.* **2019**, *7*, 10–1128. [CrossRef] [PubMed]
73. Singer, A.C.; Shaw, H.; Rhodes, V.; Hart, A. Review of Antimicrobial Resistance in the Environment and Its Relevance to Environmental Regulators. *Front. Microbiol.* **2016**, *7*, 1728. [CrossRef] [PubMed]
74. Curtis, P.D. Essential Genes Predicted in the Genome of Rubrivivax gelatinosus. *J. Bacteriol.* **2016**, *198*, 2244–2250. [CrossRef] [PubMed]
75. Vieira, S.; Huber, K.J.; Neumann-Schaal, M.; Geppert, A.; Luckner, M.; Wanner, G.; Overmann, J. Usitatibacter rugosus gen. nov., sp. nov. and *Usitatibacter palustris* sp. nov., novel members of Usitatibacteraceae fam. nov. within the order Nitrosomonadales isolated from soil. *Int. J. Syst. Evol. Microbiol.* **2021**, *71*, 004631. [CrossRef]
76. Youssef, N.H.; Rinke, C.; Stepanauskas, R.; Farag, I.; Woyke, T.; Elshahed, M.S. Insights into the metabolism, lifestyle and putative evolutionary history of the novel archaeal phylum 'Diapherotrites'. *ISME J.* **2015**, *9*, 447–460. [CrossRef]
77. Vigneron, A.; Cruaud, P.; Lovejoy, C.; Vincent, W.F. Genomic evidence of functional diversity in DPANN archaea, from oxic species to anoxic vampiristic consortia. *ISME Commun.* **2022**, *2*, 4. [CrossRef]
78. Robin, A.Y.; Brochier-Armanet, C.; Bertrand, Q.; Barette, C.; Girard, E.; Madern, D. Deciphering Evolutionary Trajectories of Lactate Dehydrogenases Provides New Insights into Allostery. *Mol. Biol. Evol.* **2023**, *40*, msad223. [CrossRef]
79. Gao, Q.; Guo, L.-N.; Li, S.-H.; Wu, W.; Ding, J.W.; Xu, H.-J.; Luo, C.-B.; Li, J.; Li, D.-Q.; Liu, Z.-Q. Biodegradation mechanism of cellulose, hemicellulose, and lignin in bacteria-dominant aerobic composting from agricultural biomass waste: A review. *Carbohydr. Polym. Technol. Appl.* **2025**, *11*, 100879. [CrossRef]
80. Leschine, S.B. Cellulose degradation in anaerobic environments. *Annu. Rev. Microbiol.* **1995**, *49*, 399–426. [CrossRef]

81. Spring, S. Kiritimatiella. In *Bergey's Manual of Systematics of Archaea and Bacteria*; Wiley Online Library: Hoboken, NJ, USA, 2023; pp. 1–6. [CrossRef]
82. Datta, R. Enzymatic degradation of cellulose in soil: A review. *Heliyon* **2024**, *10*, e24022. [CrossRef]
83. Rakitin, A.L.; Kulichevskaya, I.S.; Beletsky, A.V.; Mardanov, A.V.; Dedysh, S.N.; Ravin, N.V. Verrucomicrobia of the Family Chthoniobacteraceae Participate in Xylan Degradation in Boreal Peat Soils. *Microorganisms* **2024**, *12*, 2271. [CrossRef]
84. He, S.; Stevens, S.L.R.; Chan, L.K.; Bertilsson, S.; Glavina Del Rio, T.; Tringe, S.G.; Malmstrom, R.R.; McMahon, K.D. Ecophysiology of Freshwater Verrucomicrobia Inferred from Metagenome-Assembled Genomes. *mSphere* **2017**, *2*, 10–1128. [CrossRef] [PubMed]
85. Mirete, S.; Sánchez-Costa, M.; Díaz-Rullo, J.; González de Figueras, C.; Martínez-Rodríguez, P.; González-Pastor, J.E. Metagenome-Assembled Genomes (MAGs): Advances, Challenges, and Ecological Insights. *Microorganisms* **2025**, *13*, 985. [CrossRef] [PubMed]
86. Fierer, N.; Ladau, J.; Clemente, J.C.; Leff, J.W.; Owens, S.M.; Pollard, K.S.; Knight, R.; Gilbert, J.A.; McCulley, R.L. Reconstructing the microbial diversity and function of pre-agricultural tallgrass prairie soils in the United States. *Science* **2013**, *342*, 621–624. [CrossRef] [PubMed]
87. Bach, E.M.; Williams, R.J.; Hargreaves, S.K.; Yang, F.; Hofmockel, K.S. Greatest soil microbial diversity found in micro-habitats. *Soil Biol. Biochem.* **2018**, *118*, 217–226. [CrossRef]
88. Bach, E.M.; Hofmockel, K.S. A time for every season: Soil aggregate turnover stimulates decomposition and reduces carbon loss in grasslands managed for bioenergy. *GCB Bioenergy* **2016**, *8*, 588–599. [CrossRef]
89. Das, B.K.; Ishii, S.; Antony, L.; Smart, A.J.; Scaria, J.; Brozel, V.S. The Microbial Nitrogen Cycling, Bacterial Community Composition, and Functional Potential in a Natural Grassland Are Stable from Breaking Dormancy to Being Dormant Again. *Microorganisms* **2022**, *10*, 923. [CrossRef]
90. Liao, T.; Wang, S.; Stüeken, E.E.; Luo, H. Phylogenomic Evidence for the Origin of Obligate Anaerobic Anammox Bacteria Around the Great Oxidation Event. *Mol. Biol. Evol.* **2022**, *39*, msac170. [CrossRef]
91. Sonthiphand, P.; Hall, M.W.; Neufeld, J.D. Biogeography of anaerobic ammonia-oxidizing (anammox) bacteria. *Front. Microbiol.* **2014**, *5*, 399. [CrossRef]
92. Daims, H.; Lebedeva, E.V.; Pjevac, P.; Han, P.; Herbold, C.; Albertsen, M.; Jehmlich, N.; Palatinszky, M.; Vierheilig, J.; Bulaev, A.; et al. Complete nitrification by Nitrospira bacteria. *Nature* **2015**, *528*, 504–509. [CrossRef]
93. Koch, H.; Lücker, S.; Albertsen, M.; Kitzinger, K.; Herbold, C.; Spieck, E.; Nielsen, P.H.; Wagner, M.; Daims, H. Expanded metabolic versatility of ubiquitous nitrite-oxidizing bacteria from the genus Nitrospira. *Proc. Natl. Acad. Sci. USA* **2015**, *112*, 11371–11376. [CrossRef] [PubMed]
94. Xie, Y.; Wang, Z.; Ismail, S.; Ni, S.-Q. Long-term operation and dynamic response of dissimilatory nitrate reduction to ammonium process under low-frequency infrared electromagnetic field. *npj Clean Water* **2024**, *7*, 60. [CrossRef]
95. Zhao, Y.; Li, Q.; Cui, Q.; Ni, S.-Q. Nitrogen recovery through fermentative dissimilatory nitrate reduction to ammonium (DNRA): Carbon source comparison and metabolic pathway. *Chem. Eng. J.* **2022**, *441*, 135938. [CrossRef]
96. Phan, H.V.; Yasuda, S.; Oba, K.; Tsukamoto, H.; Hori, T.; Kuroiwa, M.; Terada, A. Active bacteria driving N2O mitigation and dissimilatory nitrate reduction to ammonium in ammonia recovery bioreactors. *ISME J.* **2025**, *19*, wraf021. [CrossRef]
97. Dahal, R.H.; Chaudhary, D.K.; Kim, D.U.; Kim, J. *Luteolibacter luteus* sp. nov., isolated from stream bank soil. *Arch. Microbiol.* **2021**, *203*, 377–382. [CrossRef]
98. Bovio-Winkler, P.; Guerrero, L.D.; Erijman, L.; Oyarzúa, P.; Suárez-Ojeda, M.E.; Cabezas, A.; Etchebehere, C. Genome-centric metagenomic insights into the role of Chloroflexi in anammox, activated sludge and methanogenic reactors. *BMC Microbiol.* **2023**, *23*, 45. [CrossRef]
99. Nagashima, S.; Shimada, K.; Vermeglio, A.; Nagashima, K.V. The cytochrome c(8) involved in the nitrite reduction pathway acts also as electron donor to the photosynthetic reaction center in Rubrivivax gelatinosus. *Biochim. Biophys. Acta* **2011**, *1807*, 189–196. [CrossRef]
100. Gan, X.; Hu, H.; Fu, Q.; Zhu, J. Nitrate reduction coupling with As(III) oxidation in neutral As-contaminated paddy soil preserves nitrogen, reduces N2O emissions and alleviates As toxicity. *Sci. Total Environ.* **2024**, *912*, 169360. [CrossRef]
101. Murphy, C.L.; Yang, R.; Decker, T.; Cavalliere, C.; Andreev, V.; Bircher, N.; Cornell, J.; Dohmen, R.; Pratt, C.J.; Grinnell, A.; et al. Genomes of Novel Myxococcota Reveal Severely Curtailed Machineries for Predation and Cellular Differentiation. *Appl. Environ. Microbiol.* **2021**, *87*, e0170621. [CrossRef]
102. Das, R.; Thatal, B.; Thakur, N.; Kumar, R.; Tamang, B. Metagenomic report of element-microbe synergy and xenobiotic detoxification in the sacred waters of Khecheopalri lake, Eastern Himalaya. *BMC Microbiol.* **2025**, *25*, 704. [CrossRef]
103. Wu, R.S.S. Eutrophication, Water Borne Pathogens and Xenobiotic Compounds: Environmental Risks and Challenges. *Mar. Pollut. Bull.* **1999**, *39*, 11–22. [CrossRef]
104. Zhang, D.; Liu, F.; Al, M.A.; Yang, Y.; Yu, H.; Li, M.; Wu, K.; Niu, M.; Wang, C.; He, Z.; et al. Nitrogen and sulfur cycling and their coupling mechanisms in eutrophic lake sediment microbiomes. *Sci. Total Environ.* **2024**, *928*, 172518. [CrossRef]

105. Nagashima, S.; Kamimura, A.; Shimizu, T.; Nakamura-Isaki, S.; Aono, E.; Sakamoto, K.; Ichikawa, N.; Nakazawa, H.; Sekine, M.; Yamazaki, S.; et al. Complete Genome Sequence of Phototrophic Betaproteobacterium Rubrivivax gelatinosus IL144. *J. Bacteriol.* **2012**, *194*, 3541–3542. [CrossRef]
106. Ramana, C.V.; Sasikala, C.; Arunasri, K.; Anil Kumar, P.; Srinivas, T.N.R.; Shivaji, S.; Gupta, P.; Süling, J.; Imhoff, J.F. *Rubrivivax benzoatilyticus* sp. nov., an aromatic, hydrocarbon-degrading purple betaproteobacterium. *Int. J. Syst. Evol. Microbiol.* **2006**, *56*, 2157–2164. [CrossRef]
107. Liu, F.Y.L.; Twible, L.E.; Colenbrander Nelson, T.E.; Whaley-Martin, K.; Yan, Y.; Arrey, J.L.S.; Warren, L.A. Microbial sulfur cycling determinants and implications for environmental impacts. *Chemosphere* **2025**, *372*, 144084. [CrossRef]